ACS EARTH AND SPACE CHEMISTRY

http://pubs.acs.org/journal/aesccq

Article

H-Abstraction from Dimethyl Sulfide in the Presence of an Excess of Hydroxyl Radicals. A Quantum Chemical Evaluation of Thermochemical and Kinetic Parameters Unveils an Alternative Pathway to Dimethyl Sulfoxide

Zoi Salta,* Jacopo Lupi, Vincenzo Barone, and Oscar N. Ventura

Cite This: *ACS Earth Space Chem.* 2020, 4, 403−419

Read Online

ACCESS | Metrics & More | Article Recommendations | Supporting Information

ABSTRACT: Elucidation of the oxidation mechanism of naturally emitted reduced sulfur compounds, especially dimethyl sulfide, plays a central role in understanding background acid precipitation in the natural environment. Most frequently, theoretical studies of the addition and H-elimination reactions of dimethyl sulfide with hydroxyl radicals are studied considering the presence of oxygen that further reacts with the radicals formed in the initial steps. Although the reaction of intermediate species with additional hydroxyl radicals has been considered as part of the global mechanism of oxidation, little if any attention has been dedicated to the possibility of reactions of the initial radicals with a second •OH molecule. In this work, we performed a computational study using quantum-chemical methods, of the mechanism of H-abstraction from dimethyl sulfide under normal atmospheric conditions and in reaction chambers at different O_2 partial pressure, including complete absence of oxygen. Additionally, important rate coefficients were computed using canonical and variational transition state theory. The rate coefficient for abstraction affords a 4.72×10^{-12} cm^3 molecule^{-1} s^{-1} value, very close to the most recent experimental one (4.13×10^{-12} cm^3 molecule^{-1} s^{-1}). According to our best results, the initial methyl thiomethyl radical was obtained at −25.2 kcal/mol (experimentally −22.4 kcal/mol), and four important paths were identified on the potential energy surface. From the interplay of thermochemical and kinetic arguments, it was possible to demonstrate that the preferred product of the reaction of dimethyl sulfide with two hydroxyl radicals is actually dimethyl sulfoxide.

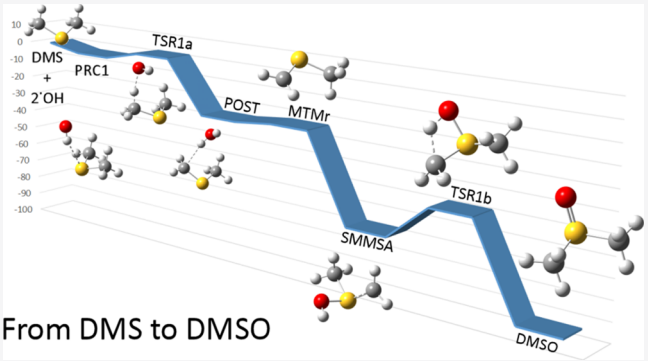

KEYWORDS: *DMS, DMSO, H-Abstraction, atmospheric chemistry, multigeneration OH oxidation, computational study*

1. INTRODUCTION

The atmospheric sulfur cycle has been the subject of intensive investigation for a long time, mostly because of the need to have a continuous assessment of the contribution of anthropogenically produced sulfur to problems such as acid rain, visibility reduction, and climate modification.[1] Field measurements have long time ago indicated that the predominant reduced sulfur compound entering the atmosphere is dimethyl sulfide (DMS).[2] In fact, ocean-emitted DMS has been suggested to play a major role in atmospheric aerosol formation and thereby cloud formation, and it has been estimated to account for approximately 60% of the total natural sulfur gases released into the atmosphere.[3,4]

For a complete understanding of the DMS oxidation mechanism, it is crucial to acquire detailed knowledge of the elementary steps that may provide general guidelines for atmospherically relevant processes. Equally important is the photochemistry of the initially formed volatile sulfur adducts and oxidation intermediates.

There is no doubt that the oxidation of DMS in the troposphere occurs primarily in the gas phase. Liquid-phase oxidation of DMS in cloud water has been discussed but there is, to the best of our knowledge, no experimental evidence proving the formation of dimethyl sulfoxide (DMSO) in cloud water. The presence of DMSO in rain and snow has, however, been documented. The extent of branching to the likely major end products sulfur dioxide, sulfur trioxide, and methanesulfonic acid (MSA) is unclear and the same applies, consequently, to the contribution of atmospheric oxidation of DMS to the formation of acid rain and the effect of DMS on

Received: November 20, 2019
Revised: February 21, 2020
Accepted: February 25, 2020
Published: February 25, 2020

https://dx.doi.org/10.1021/acsearthspacechem.9b00306
ACS Earth Space Chem. 2020, 4, 403−419

the climate. It is well known that, in solution, the oxidation of DMS by hydroperoxides leads to DMSO.[5]

In the atmosphere, DMS is believed to be removed mainly by the daytime reaction with the hydroxyl radical ($^{\bullet}OH$), by the night-time reaction with the nitrate radical ($NO_3^{\bullet}$), and by reaction with halogen oxides ($XO^{\bullet}$). In marine environments, $NO_3^{\bullet}$ levels are typically low and, as a result, DMS is expected to be destroyed primarily by $^{\bullet}OH$. In general, the initial reactions of reduced sulfur compounds with free radicals involve two pathways, abstraction and addition. The ratio between these two $^{\bullet}OH$ reaction pathways shows a strong temperature dependence.[6,7] In fact, previous studies have shown that about 70% of the DMS reacts with $^{\bullet}OH$ radicals through H-abstraction at 298 K, whereas at temperatures below 286 K, the $^{\bullet}OH$-addition pathway becomes dominant.[7−9] It is also known that the reaction is dependent on the concentration of oxygen.[10]

The reaction between DMS and $^{\bullet}OH$ radicals leads to the formation of a variety of sulfur-containing end products, with the most important being DMSO, sulfur dioxide (SO_2), MSA, sulfuric acid (H_2SO_4), and dimethylsulfone ($DMSO_2$).[10−14] The identity and yields of the final products depend on the oxidation steps of several intermediates for which a multitude of different possible reaction pathways may exist, whose importance can vary with the prevailing atmospheric conditions.[15−17] A relatively recent review and critical assessment of 20 different models and their uncertainties by Faloona[18] concluded that the standard $^{\bullet}OH$ and $^{\bullet}NO_3$ mechanisms of oxidation of DMS do not fully account for diurnal decay rates typically observed in the MBL. Moreover, Mardyukov and Schreiner[19] studied five different DMS oxidation mechanisms and compared them with nine different field measurements, concluding that no single mechanism reproduced the observations and predictions. This indicates that the mechanism of DMS oxidation is very complex and not completely understood and that the branching ratios are strongly dependent upon environmental conditions and presence of clouds. For that reason, a great number of different experimental instruments and techniques have been used to take into account all possible reaction pathways in the atmosphere, and our study will follow that example.

The kinetic information on the reaction between DMS and $^{\bullet}OH$ is currently interpreted in terms of a two-channel mechanism, involving the direct abstraction reaction (reaction R1, O_2-independent) and the reversible adduct formation (reaction R2, O_2-dependent), as shown below.[20−22]

$$^{\bullet}OH + DMS \rightarrow CH_3SCH_2^{\bullet} + H_2O \quad (R1)$$

$$^{\bullet}OH + DMS(+M) \leftrightarrow CH_3S^{\bullet}(OH)CH_3(+M) \quad (R2)$$

Detailed studies on the kinetics of the gas-phase oxidation of sulfur compounds, both organic and inorganic, can be found in many previous publications that are summarized in two important review papers.[19,22] In particular, the kinetics of the reaction of $^{\bullet}OH$ with DMS has been extensively studied using a large panel of methods.[7,12,21,23−25] Older studies provided a somewhat confusing picture of the abstraction reaction R1.[26−28] In more recent years,[7,12,29] it became clear that the results are dependent on the concentration of O_2 and NOx in the system. In particular, Hynes et al.[7] performed a comprehensive flash photolysis-resonance fluorescence investigation of this system and found that the effective rate coefficient increased as the partial pressure of oxygen was increased. Barnes et al.[13] performed a series of irradiations on DMS/ethene/H,O/N/O reaction mixtures at 760 Torr total pressure and 298 ± 3 K with O_2 partial pressures of 0, 50, 100, 155, and 760 Torr. Moreover, in Table 2, they quote nine papers, besides their own, where experiments were done in the absence of O_2 and subsequently in an excess of $^{\bullet}OH$ radicals.

The latest and most well-established kinetic data for the main reactions (addition and abstraction) of $^{\bullet}OH$ with DMS were found at two different temperatures. In one study at T = 240 K,[29] where the rate coefficient was determined as a function of pressure by using the laser-induced fluorescence analytic technique, Williams et al. found $k(R1)_{240} = (3.59 \pm 0.07) \times 10^{-12}$ cm^3 molecule^{-1} s^{-1} (at zero O_2-pressure) and $k(R2)_{240} = (5.82 \pm 1.33) \times 10^{-11}$ cm^3 molecule^{-1} s^{-1}. In another study, at T = 298 K and standard pressure P = 1 bar, Atkinson et al.[30] found $k(R1)_{298} = 4.8 \times 10^{-12}$ cm^3 molecule^{-1} s^{-1} and $k(R2)_{298} = 1.7 \times 10^{-12}$ cm^3 molecule^{-1} s^{-1}, from an expression deduced from the most accurate experimental results available. From these data, it is clear that addition predominates at lower temperatures (240 K), while at larger temperatures (298 K), abstraction takes over. However, the temperature dependence is somehow doubtful. Hynes et al.[7] determined a rate coefficient $k(R1) = (13.6 \pm 4.0) \times 10^{-12} \exp[(-332 \pm 96)/T]$ cm^3 molecule^{-1} s^{-1} in the absence of oxygen in the range of 276−397 K, independent of pressure (30−300 Torr). This means the reaction has a positive activation energy. Positive activation energies were also determined by Wine et al.,[26] Hsu et al.,[31] and Abbat et al.,[24] while only the work of Wallington et al.[32] had previously reported a negative activation energy, which would imply a transition state below the energy of the reactants and the presence of a prereactive complex.

Recently, however, Albu, Barnes et al.[16] published a study where they investigated the rate coefficient of the system at a total pressure of 760 Torr and various oxygen partial pressures, using the relative method and long path in situ Fourier transform absorption spectroscopy to monitor the disappearance rates of DMS and the reference compounds (ethene, propene and 2-methylpropene). They obtained the expression $k(R1) = (1.56 \pm 0.20) \times 10^{-12} \exp[(369 \pm 27)/T]$ cm^3 molecule^{-1} s^{-1} for zero partial pressure of oxygen in the temperature interval of 250−299 K. This means that in this most recent experimental determination, the activation energy is negative, in agreement with the previous study by Wallington et al. in 1986.[32] The study by Albu et al.[16] provided a rate coefficient at 298 K of $(5.00 \pm 1.00) \times 10^{-12}$ cm^3 molecule^{-1} s^{-1} in agreement with the previously mentioned best value recommended by Atkinson et al.[30] Later work by González-García et al.,[17] following a previous idea of El-Nahas et al.,[33] invoked the existence of two possible reaction channels for the decomposition, one through direct abstraction and another through indirect abstraction starting from a precursor complex (as postulated by Sekušak et al.[34]). Under this assumption, González-García et al.[17] proposed that the reaction is not pressure-independent (contrary to the experimental results reported by Hynes et al.[7]). They calculated that at low pressures, the temperature dependence follows an Arrhenius behavior, while at high pressures, the behavior is Arrhenius-like only at higher temperatures and reverse Arrhenius at lower ones.

Therefore, despite the maturity of the field, a large discrepancy still exists among different experimental and computational results. On the one side, several experimental

https://dx.doi.org/10.1021/acsearthspacechem.9b00306
ACS Earth Space Chem. 2020, 4, 403−419

studies employed higher NO_x concentrations[23,32,35,36] and obtained results differing from those observed at the much lower NO_x concentrations found in the atmosphere.[6,37] On the other side, it is well known that the formation of secondary organic aerosols in the atmosphere involves the multi-generation oxidation of a parent organic molecule leading to product molecules that split between the gas and particle phases. As the parent organic is consumed, usually by reaction with the $^{\bullet}$OH radical, subsequent intermediates may also react with $^{\bullet}$OH, giving rise to an evolving product distribution.[38]

Indeed, recent studies of the $^{\bullet}$OH radicals above forested regions have shown that atmospheric models underestimate in several cases the concentration of $^{\bullet}$OH radicals up to a factor of four,[39] although a recent study has suggested that typical $^{\bullet}$OH measurements may overestimate concentrations by a factor of two.[40] The problem is largely due to the complex multigenerational atmospheric chemistry involving a variety of free radical addition, abstraction, and isomerization reactions at multiple sites, with each successive oxidation step giving rise to a new generation of products.

Therefore, there are large variations in product distributions, and it is not possible to make reliable quantitative predictions of the DMS oxidation products for specific sets of atmospheric conditions. Part of the confusion is derived from the interplay of different radicals ($^{\bullet}$OH, $^{\bullet}$NO, $NO_2^{\bullet}$, and triplet O_2). For this reason, we decided to start a series of studies in which the main aspects of the reaction with each of the radicals are analyzed. This first study is devoted to the reaction of DMS with an excess of $^{\bullet}$OH radical, that is, when the first generation radicals formed can further react with other $^{\bullet}$OH molecules to give the final products either under atmospheric conditions or in laboratory experiments, in the absence of oxygen (comparable to the experiments reported by Barnes et al.[13] and Williams et al. at zero O_2-pressure[29]). Although this route was also followed by González-García et al.,[17] these authors proceeded from a termolecular complex between DMS and two hydroxyl radicals, which would require not only a large excess of $^{\bullet}$OH but also that the reaction proceeds from the well-known addition complex, further reacting with a second hydroxyl radical also added to sulfur. Under these conditions, it is more probable that the complex evolves to DMSO and water than to the abstraction complex. We will show in this paper that an alternative mechanism is possible for the generation of a methyl thiomethyl radical (MTMr), which not only is pressure-independent and gives a rate coefficient in very good agreement with the experimental results but also shows the inverse Arrhenius behavior observed by Albu et al.[16] Following these ideas, some new reaction paths are described, which may be eventually investigated experimentally.

2. COMPUTATIONAL METHODS

The potential energies of the studied compounds were analyzed using composite model chemistry methods, density functional theory (DFT), and CCSD(T) single-point calculations on the DFT-optimized geometries.

Composite model chemistry methods rely on calculations at relatively simple (and cheap) levels that are later corrected stepwise for extension of the basis set to the complete basis set (CBS) limit, for higher levels of correlation energy (MP4, CCSD(T)), and adding in some cases empirical factors to correct for dissociation energies with respect to the atoms. Available methods comprise the CBS model chemistries reported by Petersson et al.,[41,42] the Gaussian-n (Gn) methods reported by Pople and co-workers,[43] the Weizmann-n (Wn) theories reported by Martin and co-workers,[44] the focal point method[45] reported by Schuurman et al., and the "high accuracy extrapolated ab initio thermochemistry" method[46] reported by Tajti et al., among others. In particular, in this paper, we used the CBS-QB3[41,42] and G4[43] methods.

Three models rooted in the DFT were employed, namely, the M06,[47] M06-2X-D3,[47,48] and ωB97X-D[49] methods. DFT methods do not have such a large dependence on the quality of the basis set as MO methods have. However, when low stabilization energy hydrogen-bonded clusters are studied, it is reasonable to have an appraisal of the situation employing different basis sets. In our case, we chose Pople's 6-31+G(d,p) basis sets, as an example of relatively low-cost (i.e., less complete) basis set, which allowed us to perform extensive evaluation of potential energy curves and surfaces. Additionally, we used the correlation consistent basis sets of Dunning, cc-pVTZ, and aug-cc-pVQZ as examples of more complete (and costly) basis sets.

Finally, it must be pointed out that while geometries obtained at the DFT level are oftentimes sufficiently accurate, the energies are less so (a recent evaluation of the accuracy of DFT methods can be seen in the work of Mardirossian and Head-Gordon[50]). To correct this behavior, it is customary to perform single point CCSD(T) calculations on the DFT optimum geometries. This is a procedure akin to that used in composite model chemistries, where geometry optimizations and the evaluation of harmonic frequencies is performed at a lower level of calculation (B3LYP, for instance) followed by more accurate single point estimation of correlation and basis set extension effects. Thus, in this work, we added single-point CCSD(T)/cc-pVTZ energy calculations at the ωB97X-D/cc-pVTZ-optimized geometries, both for the calculation of more accurate thermochemical data and to evaluate the energy of the points on the reaction paths necessary to calculate rate coefficients. Since tight d functions are known to be important for a quantitative description of third-row atoms (here sulfur),[51] and we resorted to the jun-cc-pV(T+d)Z basis set.[52]

All geometry optimizations, energy, thermodynamic functions and frequency calculations have been performed using the Gaussian 16 system of computer codes, Revision C.01.[53] Tight thresholds were used for geometry optimizations and the ultrafine grid was used for the numerical evaluation of integrals. The standard rigid-rotor harmonic-oscillator approximation was used to compute thermochemical properties. All optimized structures were checked to be true minima by inspection of the eigenvalues of the Hessian. Heat of formation values $\Delta_f H^{\circ}_{298}$ for the important energy minima, were determined by using the methods described before and the computational thermochemistry protocol,[54] by following the procedure based on atomization energies, as outlined by Curtiss et al.[55]

All the kinetics calculations were carried out using programs of the MultiWell suite.[56−58] For the initial barrierless reaction and also for some important transition states connecting intermediate stable species or leading to final products, canonical (CTST) and variational transition state theory (VTST)[59] were employed in the following way. Constrained optimizations were carried out at a series of fixed bond lengths along each reaction path. At each point, a vibrational analysis was performed to obtain the projected vibrational frequencies of the normal vibrational modes perpendicular to the reaction path.[60] At each fixed bond distance, "trial" CTST rate coefficients as functions of the temperature T were computed

https://dx.doi.org/10.1021/acsearthspacechem.9b00306
ACS Earth Space Chem. 2020, 4, 403−419

Scheme 1. Schematic View of the Proposed Reaction Mechanism, Identifying Reactants, Intermediates, Transition States, Products, and Reaction Pathways[a]

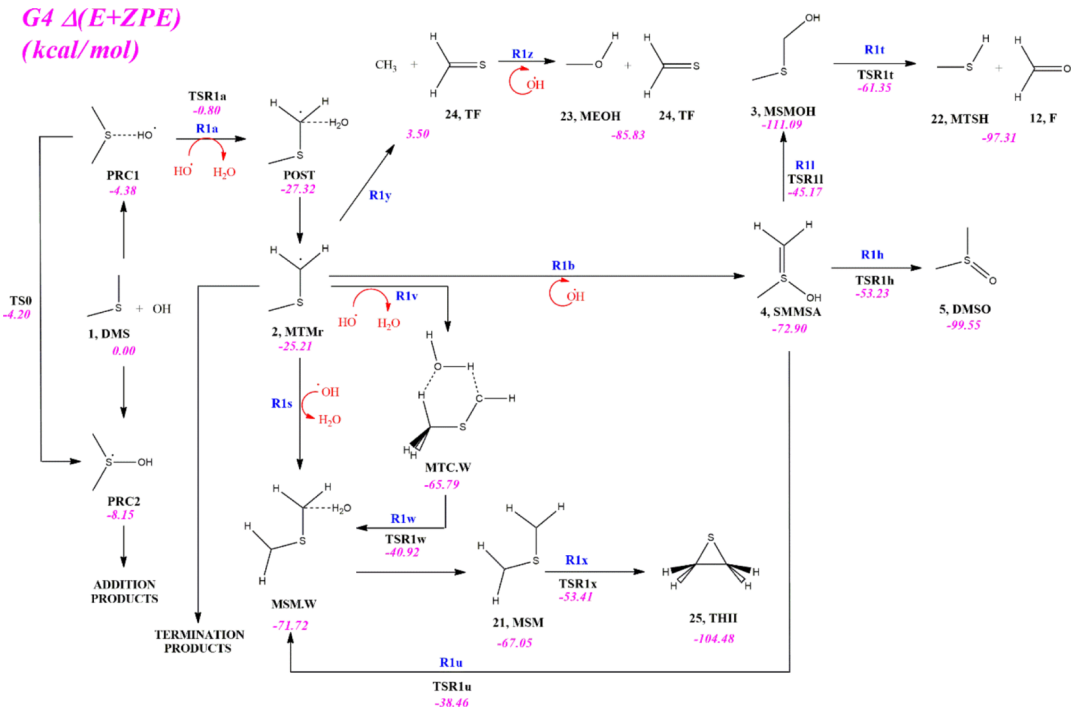

[a]G4 Δ(E + ZPE) values in kcal/mol are provided here to identify relative stabilities at a glance. Full explanations are provided in the text.

(see eq 1), based on the rotational constants, harmonic frequencies of the orthogonal degrees of freedom, potential energy, and other parameters. Thus, trial CTST rate coefficients are obtained for each temperature and at each of the fixed bond lengths. At each T, the minimum trial CTST rate coefficient is identified as the canonical VTST rate coefficient, and the structure at that position is identified as the TS. The canonical TST rate coefficient $k_{TST}(T)$ can then be expressed by

$$k_{TST}(T) = L^{\ddagger}\frac{k_B T}{h}\frac{\left(\frac{q^{\ddagger}}{V}\right)}{\left(\frac{q_C}{V}\right)}\exp\left[\frac{-E_0}{k_B T}\right] \tag{1}$$

where $L^{\ddagger}$ is the reaction path degeneracy, h is Planck's constant, T is the temperature, k_B is Boltzmann's constant, q_C/V is the partition function per unit volume for chemical species C, and E_0 is the barrier height (including zero point energy) for the reaction. The reaction path degeneracy is given by $L^{\ddagger} = \sigma_{ext}m^{\ddagger}/(\sigma_{ext}m_C)$, where σ_{ext} is the external symmetry number for molecule C and $\sigma^{\ddagger}_{ext}$ is the external symmetry number for the transition state; $m^{\ddagger}$ and m_C are the number of chiral stereoisomers of the transition state and molecule C, respectively. The partition functions are evaluated by using parameters obtained from the quantum chemistry calculations. The canonical rate coefficient for the entrance channel was calculated over the temperature range from 200 to 500 K.

3. RESULTS AND DISCUSSION

3.1. Thermodynamic Approach. In this section, we will discuss the most relevant details of the potential energy surface (PES) for the reaction of DMS with two •OH radicals. Some key geometrical parameters are shown in several figures along the main text, whereas the full set of cartesian coordinates for all reactants, intermediates, transition states, and products optimized at the ωB97X-D/aug-cc-pVQZ level are collected in the Supporting Information section. After several cycles of intermediate and transition-state calculations, the final reaction mechanism shown in Scheme 1 was derived. The stabilization energy was always taken as Δ(E + ZPE) in kcal/mol.

3.1.1. Prereactive Complexes. Two prereactive complexes were identified. The geometries of both species are shown in Figure 1. PRC2 is the most stable complex (see Table 1). It presents an interaction between sulfur and oxygen, with a secondary interaction between sulfur and the hydroxyl hydrogen (hence the SOH angle of about 100°), and can be described as a three-electron/2-center (3e⁻/2c) complex. Instead In PRC1, the primary interaction is between the hydroxyl hydrogen and sulfur, the secondary interaction is between O and the H atoms of the methyl group, and there is no interaction between sulfur and oxygen. This is a dipole−dipole complex that, to the best of our knowledge, has only been considered before by Aloisio[61] at the MP2/6-311G(d) level and by Wang and Zhang at the MP2/cc-pVTZ level.[62]

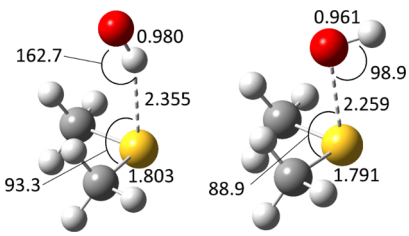

Figure 1. ωB97X-D/cc-pVTZ geometries (distances in Å and angles in degrees) of the prereactive complexes PRC1 and PRC2.

https://dx.doi.org/10.1021/acsearthspacechem.9b00306
ACS Earth Space Chem. 2020, 4, 403−419

Table 1. Relative Energies of the Prereactive Complexes PRC1 and PRC2 and the Transition State TS0 with Respect to Reactants (DMS + 2•OH) in kcal/mol[a]

		PRC1		TS0		PRC2	
		Δ(E + ZPE)	ΔH°	Δ(E + ZPE)	ΔH	Δ(E + ZPE)	ΔH°
CBS-QB3		−3.78	−4.12	−3.60	−4.09	−9.02	−9.47
G4		−4.38	−4.61	−4.20	−4.68	−8.15	−8.58
M06	6-31+G(d,p)					−12.62	−13.09
	cc-pVTZ					−10.76	−11.17
	aug-cc-pVQZ					−10.86	−11.29
ωB97X-D	6-31+G(d,p)	−4.42	−4.75	−4.56	−4.94	−10.51	−10.99
	cc-pVTZ	−4.43	−4.72	−4.58	−4.95	−9.33	−9.75
	jun-cc-pV(T+d)Z	−4.01	−4.28	−4.13	−4.52	−10.21	−10.73
	aug-cc-pVQZ	−3.91	−4.16	−4.01	−4.39	−9.89	−10.38
CCSD(T)[b]	cc-pVTZ[c]	−4.12		−3.68		−5.19	
	jun-cc-pV(T+d)Z[d]	−3.59		−3.55		−7.56	

[a]Enthalpies calculated at T = 298.15 K. PRC1 and TS0 were not found with the M06 method. [b]Single point calculations at the ωB97X-D/cc-pVTZ optimum geometries; the ZPE calculated at the level at which the geometries were optimized was added to the CCSD(T) single-point total energies to obtain the E + ZPE energies reported. [c]At the ωB97X-D/cc-pVTZ optimum geometries. [d]At the ωB97X-D/jun-cc-pV(T+d)Z optimum geometries.

PRC2 is clearly an addition complex and would react with O_2 (if present) to give DMSO. In a previous work,[17] PRC2 was also held responsible, after reaction with a second •OH radical, for some "indirect" H-abstraction, being an alternative to the direct abstraction when the •OH radical was interacting with the hydrogens of the methyl groups. In this work instead, we assumed that PRC1 would be the precursor of the abstraction of a hydrogen atom from a methyl group to give water and MTMr (see the structure of this species in Figure 2). Although it is not the main focus of this work, it may be noticed that the stabilization energy we obtained for PRC2 at the best levels of calculation is between 9 and 11 kcal/mol, to be compared with the older experimental value of 13 ± 3 kcal/mol[7] or the more recent value of 10.7 ± 2.5 kcal/mol.[21] This agreement gives further support to the accuracy of the theoretical methods we are using. Aloisio[61] found values of 12.1, 8.9, and 11.2 kcal/mol at the B3LYP, UMP2, and PMP2/6-311++G(3df,3pd) levels, respectively. Other authors got similar values.

The intrinsic reaction coordinate (IRC) from the transition state for abstraction confirms PRC1 as the initial prereactive complex (see Supporting Information section). Nonetheless, PRC1 is both difficult to locate and difficult to dissociate correctly. In fact, M06, for instance, is unable to give this structure, which is found, however, at other levels of theory (composite methods and ωB97X-D calculations). A detailed explanation of the difficulties encountered in the calculation of this complex has been included in the Supporting Information section.

PRC1 and PRC2 are separated by a very low transition state TS0 (see Figure 2). For all the methods, the total energy of TS0 is above those of both PRCs, but the situation changes when the ZPE is included. Only the CBS-QB3, G4, and CCSD(T) methods predict a barrier, albeit very small (see Table 1). The PES supporting the two reaction channels leading to the two different PRCs separated by a low ridge should be calculated at a higher level of theory to confirm our more approximate calculations.

3.1.2. Generation of MTMr. Abstraction of the hydrogen from one of the methyl groups by the •OH radical generates a complex of water and the MTMr radical, reaction R1a in Scheme 1. The enthalpies at 0 and 298 K for the initial PRC1, the transition state TSR1a, the post reactive complex (POST), and MTMr itself are shown in Table 2 with respect to the reactants.

In agreement with the experimental information,[63] as shown in Table 2 and Figure 2, MTMr is a stable structure, where the unpaired electron is shared between the sulfur atom and the methylene group. Thermochemical data indicate that the reaction to produce MTMr is exothermic by 22.4 kcal/mol, in agreement with our results. As will be shown in a later section, the standard enthalpy of formation we computed is also in good agreement with that determined experimentally.

The weakly-bound complex with water, POST, is about 3 kcal/mol more stable. The presence of this ancillary water molecule has not been taken into account in the present study, where all further reactions were started from MTMr itself. However, it is noticed that in several cases,[64−68] the interaction of radicals of atmospheric interest with water may affect their structure and reactivity. We display in Figure 3 the Laplacian of the density for POST, which shows the interaction of water with the CH_2 residue on one side and the methyl group on the other. The spin distribution is also shown in this figure for both POST and MTMr. Clearly there is very little electron transfer from MTMr to water, and the unpaired electron is contained in an antibonding π^* orbital of the S═CH_2 fragment. Moreover, given the reaction exothermicity of the abstraction, it is likely that it will almost instantaneously dissociate. Equilibration with water vapor may however be a secondary process. Therefore, we felt justified to study the reactions starting from the isolated MTMr instead of the water complex.

The activation energy for reaction R1a has been estimated experimentally to be smaller than 1 kcal/mol,[7] but this is a subject that provokes discrepancies because Arrhenius expressions obtained in different experiments predict positive or negative activation energies in the absence of oxygen. Our best theoretical results for the barrier at room temperature vary between 1.8 and 3.4 kcal/mol, confirming its small height. We will discuss the kinetic implications of this fact in a specific section.

3.1.3. Reactions of MTMr with a Second •OH Radical. The second generation reaction of the initial MTMr radical with another •OH species may follow different paths. Conceptually, one could think of at least four alternative mechanisms.

https://dx.doi.org/10.1021/acsearthspacechem.9b00306
ACS Earth Space Chem. 2020, 4, 403−419

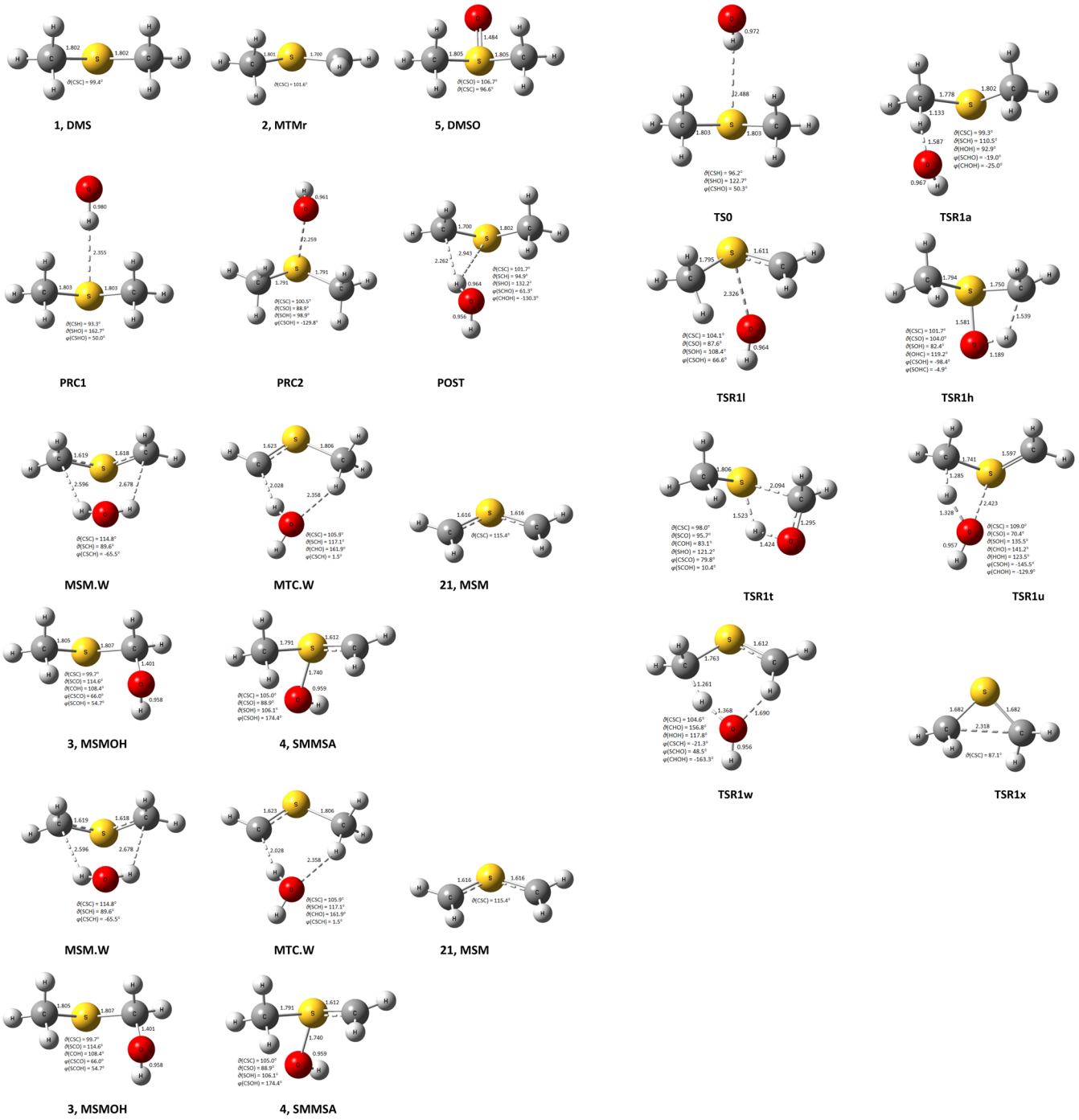

Figure 2. Most important geometrical parameters of reactants, intermediates, products, and transition states investigated in this work at the ωB97X-D/aug-cc-pVQZ level. Distances are in Å, angles in degrees.

In the first place, taking into account the fact that experimentally it was proven that MTMr is produced near the unimolecular dissociation threshold to $^{\bullet}CH_3$ + CH_2S[63] (reaction R1y), one could envisage a termination reaction of both radicals, $^{\bullet}OH$ and $^{\bullet}CH_3$. The end products would then be CH_3OH (MEOH) + CH_2S (TF), as shown for reaction R1z in Scheme 1. The average of our best theoretical results (see the Supporting Information section for detailed tables of all energies) gives a $\Delta_r H_{298}$ of −84.2 kcal/mol, about 60 kcal/mol more stable than the sum of MTMr and $^{\bullet}OH$. Free energies are also very negative, showing that this is a spontaneous reaction. No transition state was found for this reaction (which, if any, would resemble a S_N2 Walden inversion on $^{\bullet}CH_3$ to expel CH_2S), and the data suggest that this channel proceeds without any barrier, as shown in Figure 4, for the scan of the energy as a function of the C−S distance. Taking into account the stability of MTMr with respect to the reactants, the pseudobarrier for the couple R1y/R1z reactions would be about 30 kcal/mol (the best results are 30.6 and 33.1 kcal/mol for M06 and ωB97X-D, respectively, with the aug-cc-pVQZ basis set and 27.3 kcal/mol at the CCSD(T)/cc-pVTZ//ωB97X-D/cc-pVTZ level). Our value at the CCSD(T)/cc-pVTZ//ωB97X-D/cc-pVTZ level (27.3 kcal/mol) agrees fairly well with the experimental one, 24.8 kcal/mol.[63]

https://dx.doi.org/10.1021/acsearthspacechem.9b00306
ACS Earth Space Chem. 2020, 4, 403−419

Table 2. Energetics of Reaction R1a (See Scheme 1) for the Generation of the Free MTMr Radical[a]

		PRC1		TSR1a		POST		MTMr		barrier
		$\Delta(E + ZPE)$	$\Delta H°$	$\Delta(E + ZPE)$	$\Delta H°$	$\Delta(E + ZPE)$	$\Delta H°$	$\Delta(E + ZPE)$	$\Delta H°$	$\Delta(E + ZPE)$
CBS-QB3		−3.78	−4.12	−0.21	−0.93	−27.28	−27.32	−25.21	−24.80	3.57
G4		−4.38	−4.61	−0.80	−1.56	−27.32	−27.41	−25.21	−24.80	3.58
M06	6-31+G(d,p)			−4.79	−5.52	−27.28	−27.22	−24.13	−24.02	2.42
	cc-pVTZ			−4.45	−5.37	−27.33	−27.32	−23.63	−23.51	
	aug-cc-pVQZ			−3.62	−4.42	−27.78	−28.05	−25.11	−24.99	
M06-2X-D3	6-31+G(d,p)	−8.99	−9.62	−0.50	−1.26	−25.05	−24.95	−21.14	−20.68	8.49
	cc-pVTZ	−4.82	−5.26	−1.17	−2.05	−27.24	−27.10	−22.86	−22.35	3.65
	jun-cc-pV(T+d)Z	−4.08	−4.52	−0.73	−1.53	−27.66	−27.47	−24.41	−23.86	3.35
	aug-cc-pVQZ	−3.77	−4.24	−0.69	−1.48	−27.55	−27.36	−24.41	−23.83	3.08
ωB97X-D	6-31+G(d,p)	−4.42	−4.75	−2.00	−2.72	−25.65	−25.59	−22.78	−22.65	2.42
	cc-pVTZ	−4.43	−4.72	−2.43	−3.25	−26.68	−26.64	−23.20	−22.49	2.00
	jun-cc-pV(T+d)Z	−4.01	−4.28	−1.80	−2.52	−27.32	−27.17	−24.78	−24.18	2.21
	aug-cc-pVQZ	−3.91	−4.16	−1.68	−2.40	−27.24	−27.07	−24.81	−24.19	2.23
CCSD(T)[b]	cc-pVTZ[c]	−4.12		1.06		−25.24		−22.31		5.18
	jun-cc-pV(T+d)Z[d]	−3.59		0.94		−26.20		−23.93		4.53

[a]All energies with respect to the reactants (DMS + 2•OH) in kcal/mol. Enthalpies calculated at T = 298.15 K. [b]Single point calculations at the ωB97X-D/cc-pVTZ optimum geometries; the ZPE calculated at the level at which the geometries were optimized was added to the CCSD(T) single-point total energies to obtain the E + ZPE energies reported. [c]At the ωB97X-D/cc-pVTZ optimum geometries. [d]At the ωB97X-D/jun-cc-pV(T+d)Z optimum geometries.

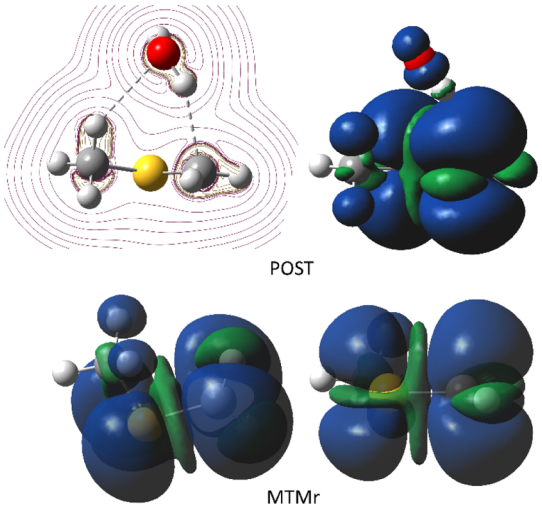

Figure 3. Laplacian of the density and spin distribution for the MTMr·H_2O complex (POST), upper images, and spin distribution for MTMr in two different views, lower images.

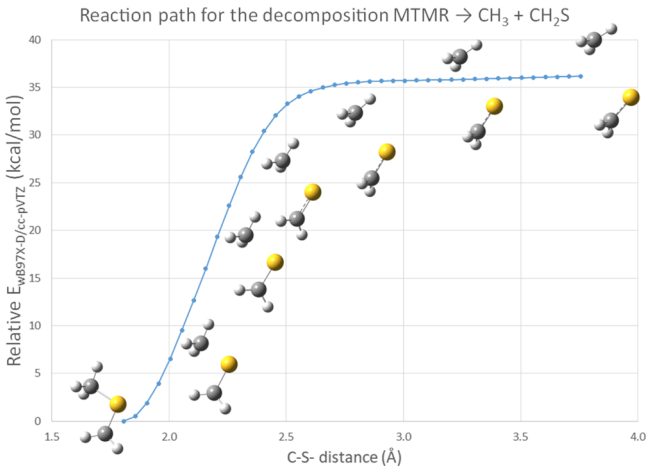

Figure 4. Total energy (w/o ZPE) for the breaking of the C−S bond in the MTMr radical.

A second alternative is indicated as reaction R1s in Scheme 1. It is basically the approach of a second •OH radical to the methyl group in MTMr, producing another H-abstraction and a complex we have called dimethylene sulfide water complex (MSM·W) in Scheme 1 (see Figure 2). This route has several complications. On one side, when both radicals are far apart, the system would behave either as a triplet or open-shell singlet. If the reaction would proceed on the triplet surface, then a spin-forbidden crossing would be necessary to obtain the final closed shell MSM·W complex. If, instead, the reaction proceeds on the open-shell singlet surface until it crosses the closed-shell singlet one, multiconfigurational calculations are needed to represent each point on the path. Our attempts to follow this reaction as an open-shell singlet using DFT and starting from the optimum geometry and electronic density of the triplet-state minimum (see the Supporting Information section for the details and justification of this approach) failed. All attempts ended up giving structure MTC·W (see Figure 2), following a barrierless path R1v.

As can be seen from its structure, MTC·W is a closed-shell methyl thiocarbene strongly bound to a water molecule. This water molecule acts as a hydrogen bridge to transfer one hydrogen atom from the methyl to the carbene fragment, reaction R1w, resulting in MSM·W along an exothermic multistep path. MSM·W can lose the attached water and cyclicize with relative easiness, giving the very stable thiirane, reaction R1x. Two transition states are involved in this reaction path, TSR1w and TSR1x, and the average values of the barriers are 25.6 and 18.6 kcal/mol, respectively. Obviously then, the rate-limiting transition state is TSR1w, and the barrier is 16% lower, approximately, than that for the dissociation into thioformaldehyde (TF) and methyl radical, which might later react with another •OH radical. The reaction enthalpies are also in favor of the larger stability of thiirane (THII) (see Table 3).

Finally, there is the obvious path for the termination reaction when the oxygen of the •OH radical interacts with the sulfur or

https://dx.doi.org/10.1021/acsearthspacechem.9b00306
ACS Earth Space Chem. 2020, 4, 403−419

Table 3. All Energies of the Species Involved in Reactions R1v/R1w/R1x and R1 with Respect to the Reactants (DMS + 2•OH) in kcal/mol[a]

		MTMr		MTC·W		TSR1w		MSM·W	
		Δ(E + ZPE)	ΔH°	Δ(E + ZPE)	ΔH°	Δ(E + ZPE)	ΔH°	Δ(E + ZPE)	ΔH°
CBS-QB3		−25.21	−24.80	−67.13	−67.54	−41.54	−42.90	−72.75	−72.48
G4		−25.21	−24.80	−65.79	−66.22	−40.92	−42.34	−71.72	−71.61
M06	6-31+G(d,p)	−24.13	−24.02	−65.19	−65.36	−40.73	−41.92	−63.66	−63.56
	cc-pVTZ	−23.63	−23.51	−64.38	−64.68	−38.61	−39.88	−66.00	−66.04
	aug-cc-pVQZ	−25.11	−24.99	−65.96	−66.11	−40.29	−41.44	−68.65	−68.44
ωB97X-D	6-31+G(d,p)	−22.78	−22.65	−58.64	−58.84	−35.36	−36.60	−57.24	−57.17
	cc-pVTZ	−23.20	−22.49	−59.39	−59.69	−34.57	−35.92	−61.96	−61.85
	jun-cc-pV(T+d)Z	−24.78	−24.18	−62.18	−62.31	−37.98	−39.22	−65.99	−66.35
	aug-cc-pVQZ	−24.81	−24.19	−61.96	−62.09	−37.41	−38.65	−65.20	−65.03
CCSD(T)[b]	cc-pVTZ[c]	−22.31		−60.97		−34.23		−64.21	
	jun-cc-pV(T+d)Z[d]	−23.93		−63.90		−38.52		−67.94	
		MSM		TSR1x		THII		SMMSA	
		Δ(E + ZPE)	ΔH°	Δ(E + ZPE)	ΔH°	Δ(E + ZPE)	ΔH°	Δ(E + ZPE)	ΔH°
CBS-QB3		−70.93	−70.74	−54.98	−55.23	−106.01	−106.37	−73.61	−74.68
G4		−67.05	−70.14	−53.41	−53.66	−104.48	−104.85	−72.90	−74.01
M06	6-31+G(d,p)	−61.41	−61.17	−44.90	−45.12	−105.95	−106.31	−64.73	−65.83
	cc-pVTZ	−63.12	−62.92	−44.85	−45.08	−104.83	−105.20	−67.47	−68.59
	aug-cc-pVQZ	−66.52	−66.31	−47.37	−47.59	−106.47	−106.82	−69.77	−70.88
ωB97X-D	6-31+G(d,p)	−54.82	−54.65	−36.57	−36.81	−99.11	−99.46	−60.16	−61.28
	cc-pVTZ	−58.79	−58.65	−38.52	−38.77	−98.74	−99.09	−64.36	−65.50
	jun-cc-pV(T+d)Z	−63.62	−63.49	−42.13	−42.38	−100.56	−100.90	−68.95	−70.10
	aug-cc-pVQZ	−62.98	−62.83	−41.87	−42.11	−101.18	−101.52	−67.59	−68.72
CCSD(T)[b]	cc-pVTZ[c]	−64.21		−45.50		−99.53		−63.07	
	jun-cc-pV(T+d)Z[d]	−67.94		−48.75		−101.42		−68.24	

[a]Enthalpies calculated at T = 298.15 K. [b]Single point calculations at the ωB97X-D/cc-pVTZ optimum geometries; the ZPE calculated at the level at which the geometries were optimized was added to the CCSD(T) single-point total energies to obtain the E + ZPE energies reported. [c]At the ωB97X-D/cc-pVTZ optimum geometries. [d]At the ωB97X-D/jun-cc-pV(T+d)Z optimum geometries.

carbon atoms in the S═CH_2 double bond. Two stable species were located, which we called *S*-methyl-methanesulfenic acid (SMMSA) and methanesulfenyl methanol (MSMOH) and were fully described in a previous publication.[69]

The relative energies of SMMSA(s) with respect to the reactants at all levels of calculation used in this study are also collected in Table 3. If, as suggested by the study of the triplet analogue, there is no barrier (or an exceedingly small one) for reaction R1b, then the formation of SMMSA will be thermodynamically as favorable (or even more) as the formation of MTC·W through the (presumably) barrierless reaction R1v. The reaction path R1y/R1z would not compete because even if the MEOH + TF products are more stable than either SMMSA or MTC·W, the dissociation to methyl radical and TF requires extra energy.

3.1.4. Intermediate Closed Shell Species. Some of the species that are predicted computationally to be formed by the second generation reaction of MTMr with the hydroxyl radical are well known (TF, methanol, thiirane), while others are more exotic and seldom described, if ever, in previous publications. In this section, we will describe two of these species, the intermediates MTC and MSM. Optimum geometries of the species are shown in Figure 2.

MTC is a carbenoid structure, whose putative existence depends on the tightly bound water molecule linking the CH_3 and CH residues. As said before, the water molecule acts as a hydrogen bridge for the migration of one H from the first to the latter, giving MSM·W, the water complex of MSM. The closed-shell structure is very stable with respect to the reactants (about −66 kcal/mol at the G4 level), but it should probably be investigated further using multireference methods. As it is obvious from the structure, two open-shell configurations are possible, a singlet and a triplet, if a double bond is formally drawn between C and S, allowing the coexistence of individual uncoupled electrons on both atoms. Although we have not further investigated this aspect, the route leading to the very stable THII is of considerable interest and will be the subject of future studies.

MSM is a closed-shell planar structure, where two methylene groups are bound to the central sulfur. It is one of the minima on the [SC_2H_4] PES, where one finds also thioacetaldehyde, ethenethiol, and thiirane. From a purely formal point of view, one could draw double bonds between the sulfur and the terminal methylene groups, satisfying then the valences of both carbons. However, the situation is more complicated. CH_2 is isoelectronic with oxygen, and thus, MSM is isoelectronic with SO_2, the electronic structure of which was recently studied by Lan, Wheeler, and Houk.[70] They performed a study of the reactivity of SO_2 in comparison with ozone (which is valence isoelectronic) and found that the very different reactivity among them can be explained by the prevalence of a dritterionic structure in the former (i.e., two positive charges on sulfur and one negative charge on each of the carbons). While the diradical valence bond structure of O_3 has a weight of 49.5% on the global description of this molecule, it has a weight of only 2.4% in SO_2. The zwitterionic ($O{=}S^+{-}O^-$, $O^-{-}S^+{=}O$) has a weight 36.0%, and the dritterionic structure ($O^-{-}S^{2+}{-}O^-$) has a weight of 59.8%. Thus, while O_3

https://dx.doi.org/10.1021/acsearthspacechem.9b00306
ACS Earth Space Chem. 2020, 4, 403−419

Table 4. Energetics of the End Products Arising from SMMSA and the Transition States Involved with Respect to the Reactants (DMS +2•OH) in kcal/mol[a]

		SMMSA		TSR1h		DMSO		TSR1u		MSM·W	
		Δ(E + ZPE)	ΔH°	Δ(E + ZPE)	ΔH°	Δ(E + ZPE)	ΔH°	Δ(E + ZPE)	ΔH°	Δ(E + ZPE)	ΔH°
CBS-QB3		−73.61	−74.68	−54.16	−55.66	−101.25	−102.50	−39.04	−40.14	−72.75	−72.48
G4		−72.90	−74.01	−53.23	−54.74	−99.55	−100.83	−38.46	−39.65	−71.72	−71.61
M06	6-31+G(d,p)	−64.73	−65.83	−45.87	−47.38	−88.95	−90.25	−36.58	−37.51	−63.66	−63.56
	cc-pVTZ	−67.47	−68.59	−50.10	−51.63	−93.65	−94.95	−35.09	−36.15	−66.00	−66.04
	aug-cc-pVQZ	−69.77	−70.88	−51.84	−53.35	−96.95	−98.25	−37.43	−38.35	−68.65	−68.44
ωB97X-D	6-31+G(d,p)	−60.16	−61.28	−40.62	−42.15	−85.39	−86.71	−29.98	−30.96	−57.24	−57.17
	cc-pVTZ	−64.36	−65.50	−46.28	−47.82	−91.18	−92.50	−30.31	−31.48	−61.96	−61.85
	jun-cc-pV(T+d)Z	−68.95	−70.10	−50.11	−51.65	−97.25	−99.20	−34.25	−35.32	−65.99	−66.35
	aug-cc-pVQZ	−67.59	−68.72	−48.92	−50.44	−95.30	−96.63	−33.60	−34.65	−65.20	−65.03
CCSD(T)[b]	cc-pVTZ[c]	−63.07		−45.32		−88.46		−29.95		−64.21	
	jun-cc-pV(T+d)Z[d]	−68.24		−49.52		−95.00		−34.99		−67.94	

		TSR1l		MSMOH		TSR1t		MTSH + F	
		Δ(E + ZPE)	ΔH°	Δ(E + ZPE)	ΔH°	Δ(E + ZPE)	ΔH°	Δ(E + ZPE)	ΔH°
CBS-QB3		−45.17	−46.40	−113.35	−114.60	−63.75	−64.95	−99.52	−99.71
G4		−45.17	−46.40	−111.09	−112.34	−61.35	−62.60	−97.31	−97.52
M06	6-31+G(d,p)	−40.73	−41.89	−112.04	−113.26	−65.56	−66.83	−97.18	−97.38
	cc-pVTZ	−37.24	−38.46	−111.32	−112.55	−65.64	−66.90	−98.99	−99.18
	aug-cc-pVQZ	−40.60	−41.73	−111.36	−112.56	−65.20	−66.43	−98.62	−98.79
ωB97X-D	6-31+G(d,p)	−34.11	−35.33	−108.71	−109.96	−59.45	−60.76	−93.42	−93.59
	cc-pVTZ	−31.59	−32.86	−108.52	−109.76	−60.45	−61.78	−95.04	−95.20
	jun-cc-pV(T+d)Z	−36.55	−37.73	−105.33	−110.14	−60.73	−62.04	−95.13	−95.28
	aug-cc-pVQZ	−36.06	−37.24	−109.42	−110.60	−60.98	−62.27	−95.47	−95.61
CCSD(T)[b]	cc-pVTZ[c]	−32.66		−107.25		−59.03		−94.91	
	jun-cc-pV(T+d)Z[d]	−39.60		−108.25		−60.09		−95.12	

[a]Enthalpies calculated at T = 298.15 K. Some of the species have been repeated for clarity. [b]Single point calculations at different optimum geometries; the ZPE calculated at the level at which the geometries were optimized was added to the CCSD(T) single-point total energies to obtain the E + ZPE values reported. [c]At the ωB97X-D/cc-pVTZ optimum geometries. [d]At the ωB97X-D/jun-cc-pV(T+d)Z optimum geometries.

https://dx.doi.org/10.1021/acsearthspacechem.9b00306
ACS Earth Space Chem. 2020, 4, 403−419

participates in radical reactions, SO_2 behaves differently. Considering then that MSM is isoelectronic with SO_2, one could expect a similar behavior. We performed the calculation of SO_2 at the same ωB97X-D/aug-cc-pVQZ level we used for MSM and compared the Mulliken charge distribution as a fast procedure to compare the weight of the dritterionic structure. While the charge on sulfur in SO_2 is +1.54, it is 0.96 in MSM. The charges on O and CH_2 are −0.77 and −0.48, respectively, (in the last case composed of a negative −0.98 charge on carbon and a joint positive charge of 0.50 on the hydrogens). Thus, at this simple level, MSM resembles SO_2 and would probably exhibit similar characteristics, although perhaps the diradical structure may have a larger weight. The cyclization of MSM, to give thiirane, requires the simultaneous rotation of the CH_2 groups, the elongation of the S−C bonds and, finally, the closure of the ring. This process is not as energetically costly as it would look like, with a barrier of about 14 kcal/mol (at the G4 level), smaller for instance than the one needed to transform MTC·W into MSM·W. A more in depth study of this relationship is under way and will be published elsewhere.

The other two interesting structures, SMMSA and MSMOH, have been reported and studied in depth in our previous publication.[69] In the following, we will only describe the reactions that may occur having these species as reactants.

3.1.5. Products from SMMSA. Three reaction channels are open for SMSSA, as can be seen in Scheme 1, where the products are MSM·W (transition state TSR1u), DMSO (transition state TSR1h), and MSMOH (transition state TSR1l). The energies of these species have been collected in Table 4.

The transition state TSR1h, leading to DMSO, is the lowest of the three, making then the formation of DMSO by an O−C hydrogen shift, the most probable process, followed by the isomerization to MSMOH. As seen in the table, MSMOH is actually more stable than all the other species, but the transition state for the process requires a S−C OH-shift, which is more energy demanding than the simple H-shift, even if tunneling is not taken into account. If MSMOH would be formed, it would have the possibility to dissociate into methanethiol (MTSH) and formaldehyde (F) (analogously to the process of formation of TF and methanol in reactions R1y/R1z), but the transition state is too high for any effective conversion.

3.1.6. Dimerization Products. As can be seen in Scheme 1, whenever the hydroxyl radical is not in excess, MTMr will be produced but will not react further with additional $^{\bullet}$OH. Taking into account the different possibilities of the reaction, at least three compounds may be obtained, depending on whether a C−C, C−S, or S−S bond is formed. We have investigated these structures at the ωB97X-D/6-31+G(d,p) level and found them, as shown in Figure 5. Isomer 1 is the most stable of the three, but even in this case, the dimerization is not competitive with reactions R1v or R1b if enough hydroxyl groups are present (the isomers are less stable than either MTC·W or SMMSA at the same theoretical level). If few hydroxyl groups are present, MTMr will also be scarce and the probability of two MTMr molecules colliding is lower. Then, the probability of dissociation by collision with other molecules of DMS increases because experimentally, it was shown to be a phenomenon occurring in the millisecond time scale. Hence, one would expect that unimolecular dissociation predominates at small $^{\bullet}$OH concentration, followed by dimerization when more hydroxyl radicals are present, and

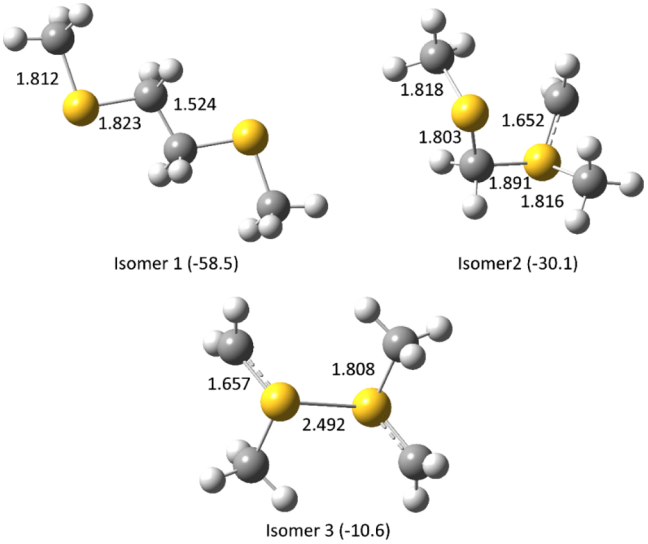

Figure 5. Structure of the three isomers for the product of the dimerization of two MTMr radicals. Most important bond distances in Å and relative $\Delta(E + \mathrm{ZPE})$ energies in kcal/mol with respect to 2DMS + 2$^{\bullet}$OH are shown at the ωB97X-D/6-31+G(d,p) level.

starts giving other products when the hydroxyl concentration is large enough.

It is clear that the stability of the dimer is larger when both sulfur atoms are in the S(II) state of oxidation. The disulfide bridge in isomer 3, even if normally very stable, produces the least stable isomer because both sulfurs are in the S(IV) oxidation state, in order to support the structure of the methylene substituents. Because of the marginal role played by these structures in the problem at hand, we did not investigate these molecules at more sophisticated levels of theory.

3.1.7. Energetics and General Reaction Scheme. Collecting all the previous results, we obtain the energy diagram shown in Figure 6. This diagram has been built using the G4 $\Delta(E + \mathrm{ZPE})$ energies, but as can be seen from the tables we presented already and the full data collected in the Supporting Information section, all the theoretical levels give a similar qualitative picture, with quantitative differences that do not affect the general conclusions. This is shown in Figure SMF10 in the Supporting Information section.

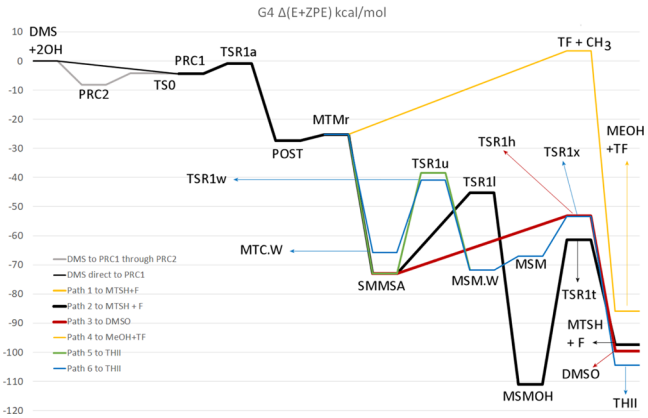

Figure 6. Schematic diagram of the different reaction paths for the reaction of DMS with two hydroxyl radicals at the G4 level of calculation. Names of the structures correspond to those shown in Scheme 1. Energies are in kcal/mol.

https://dx.doi.org/10.1021/acsearthspacechem.9b00306
ACS Earth Space Chem. 2020, 4, 403−419

Table 5. Standard Enthalpies of Formation (298.15 K, 1 atm) of the Species Involved in the Studied Reaction Paths (in kcal/mol)[a]

	CBS-QB3		G4		experimental	
species	HOF	error	HOF	error	HOF	refs
1.DMS	−7.93	1.0	−7.46	1.5	−8.96	72
2.MTMr	33.76	−1.8	33.23	−2.3	35.56	73
5.DMSO	−33.99	2.0	−33.02	3.0	−35.97	74
12.F	−26.63	1.1	−26.11	1.6	−27.70	75
22.MTSH	−4.57	0.9	−3.61	1.8	−5.45	76
23.MEOH	−47.11	1.9	−46.32	2.7	−49.00	[b]AVG
24.TF	27.61	−0.6	27.95	−0.3	28.20	77
25.THII	18.58	−1.1	18.66	−1.0	19.70	78
3.MSMOH	−46.09		−44.53			
4.SMMSA	−6.16		−6.20			
21.MSM	54.31		53.37			
r.m.s.e		1.4		2.0		

[a]Experimental and/or accurate theoretical values are reported when known, and the signed errors are calculated with respect to the most accurate experimental values available. Root mean square errors (r.m.s.e) for each method have been determined as an average of the errors for each of the species whose experimental values are known. [b]AVG = value is an average of selected values.

The main paths leading to the preferred products have been highlighted with bold lines in this figure. Several remarks are in order. In the first place, it is noticeable that the unimolecular decomposition to CH_3 + TF is unfavorable, possibly occurring only at very low •OH concentrations (dimerization products of MTMr have not been plotted in this image). In the second place, the reaction path leading to SMMSA is more favorable than that leading to MTC·W (and ultimately to THII) so that, even if THII is thermodynamically favored, it has a low probability to be produced. Finally, two paths can be followed starting from SMMSA, one of them leading to the very stable MSMOH (which later might decompose to MTSH + F) and the other directly to the DMSO product. Although MSMOH is the most stable species, the transition state TSR1l which leads to SMMSA is higher in energy than the transition state TSR1h leading to DMSO. Therefore, we can conclude that the reaction of DMS with excess •OH would end up giving DMSO as an observable product. Notice that formerly it was assumed that DMSO could be obtained only from the addition of •OH to DMS and later reaction with O_2. However, we have shown here that DMSO can also be obtained from the abstraction path, when excess •OH is present, and minimize in that way the existing discrepancies between devised model simulations and field observations of the DMS oxidation mechanisms.[71]

3.1.8. Enthalpies of Formation. Because most of the structures on the reaction paths studied involve products which are well known experimentally, we pursued a determination of their standard enthalpies of formation (HOF) $\Delta_f H^o_{298}$ as an indicator of the accuracy of the methods we have used in this paper on one side and on the other side as a way to obtain an estimation of the experimentally unknown enthalpies of formation of the three species MSM, MSMOH, and SMMSA. The enthalpies of formation were determined using the atomization energies[54,55] for each of the two composite methods used in this work. The results have been collected in Table 5.

The main conclusion from the results in Table 5 is that both methods afford results within chemical accuracy (<2 kcal/mol) on average. Quite surprisingly, the CBS-QB3 method (the simplest one) is able to produce errors below 2 kcal/mol for each of the individual species. Taking into account the average value and the error as twice the average r.m.s.e. for the two methods, our best estimates for the heats of formation of the three species are

$$\Delta_f H^o_{298}(\text{MSMOH}) = -45.3 \pm 3.3 \text{ kcal/mol}$$

$$\Delta_f H^o_{298}(\text{SMMSA}) = -6.2 \pm 3.3 \text{ kcal/mol}$$

$$\Delta_f H^o_{298}(\text{MSM}) = 53.8 \pm 3.3 \text{ kcal/mol}$$

Notice that the negative enthalpy of formation of SMMSA comparable to those of DMS or MTSH implies that this species might be formed, under suitable conditions. On the contrary, the large positive enthalpy of formation of MSM, much larger than that of THII, makes this compound probably difficult to form under normal conditions.

3.2. Kinetic Evaluation. The first recommendation for the rate coefficient for reaction R1 at 298 K from the review by DeMore et al.[79] based largely on the measurements in refs[7,21,24,31] is 5×10^{-12} cm^3 $molecules^{-1}$ s^{-1}. Slightly lower values can be found in the reviews by Atkinson,[80] Atkinson et al.,[30] and Tyndall and Ravishankara.[14] Quantum chemical calculations of the rate coefficient for the abstraction of an H atom from DMS have been reported by Sekušak et al.,[34] El-Nahas et al.,[33] and González-García et al.[17] The rate coefficients calculated at different computational levels reported by Sekušak et al.[34] starting from a prereactive complex gave values varying from 2.68 to 0.16×10^{-12} cm^3 $molecule^{-1}$ s^{-1} using MBPT(2) and CCSD(T) methods, respectively, with a commonly observed peculiarity in computational kinetics: the more sophisticated the quantum chemical method the more distant the computed value from its experimental counterpart. The calculations reported by El-Nahas et al.[33] at the PMP2/6-311++G(2df,2pd)//MP2/6-311++G(d,p) level afforded a best value of 1.1×10^{-12} cm^3 $molecule^{-1}$ s^{-1}, four to five times smaller than the experimental one. González-García et al.,[17] assuming direct and indirect H-abstraction, determined a value of 3.02×10^{-12} cm^3 $molecule^{-1}$ s^{-1} using the MPW1K/MG3S method to obtain geometries and the CCSD(T)/IB method to calculate energies (IB refers to a kind of CBS extrapolation using only cc-pVDZ and cc-pVTZ single point energies). Their value is notoriously better than the others, but it depends on the existence of a pressure-

https://dx.doi.org/10.1021/acsearthspacechem.9b00306
ACS Earth Space Chem. 2020, 4, 403−419

dependent path, in disagreement with experimental observations (see, for instance, Hynes et al.[7] or Williams et al.[81]).

As referred in the Computational Methods section, we did calculations at different levels. First, we used DFT methods (ωB97X-D and M06-2X-D3 functionals) and composite model chemistry methods (CBS-QB3 and G4) to obtain the geometries of the minima and transition states. The geometries and projected frequencies at different points of the scan and IRC necessary to study the reaction channels of both elementary reactions (formation of PRC1 from the reactants and passage over the transition state TSR1a to give the MTMr + H_2O products) were obtained by using only DFT methods. In order to obtain a better evaluation of the energies, single point CCSD(T) calculations were done on the optimized geometries obtained with the DFT methods, and both canonical TST and VTST calculations were performed with the data collected. The results are shown in Table 6.

Different from previous approaches, we used the dipole−dipole prereactive complex PRC1 as the initial complex, and not PRC2, as has been previously attempted. This is important to understand why the values we obtained for the rate coefficient [3.00−4.72] × 10^{-12} cm^3 $molecule^{-1}$ s^{-1} (M06-2X-D3 method with different basis sets) are in excellent agreement with the most recent value reported by Williams et al.,[81] 4.13 × 10^{-12} cm^3 $molecule^{-1}$ s^{-1}, determined using their eq IV for the dependence of the rate coefficient with the temperature and selecting T = 298.15 K. It is important to notice that because we do not include the addition complex in our mechanism, there is no pressure dependence, in agreement with the experiment.[7,81]

At the other temperature at which careful experimentation was employed (about 240 K), Williams et al.[29] obtained a value of (3.59 ± 0.7) × 10^{-12} cm^3 $molecule^{-1}$ s^{-1} which is comparable to our value of 3.78 × 10^{-12} cm^3 $molecule^{-1}$ s^{-1} (CTST:M06-2X-D3/jun-cc-pV(T+d)Z level). This leads to another point of the study; it is not only important to obtain a good match between the theory and the experiment at 298 K but also to take into account the temperature dependence, as we have already mentioned. In Figure 7, we have plotted the equations available in the literature for the dependence of the rate coefficient with the temperature[7,17,24,30−32,82] and compared them with our CTST values.

Two things are immediately obvious. On the one side, all curves have a crowding point in the vicinity of room temperature. Although the span is still large, the set of all the graphs has its smallest dispersion. On the other side, it is clear that the various methods predict different behaviors with the temperature. The most recent experimental measurements, reported by Albu, Barnes et al.,[16] have the same trend as our CBS-QB3 and M06-2X-D3 calculations, which implies a negative activation energy, meaning that the transition state is under the energy of the reactants, so that the barrier is related to the existence of a prereactive complex. The measurements reported by Wallington et al.[32] support this view only partially. The activation energies are −369 ± 27[35] and −130 ± 102 K,[32] while our values derived from the Arrhenius plot at the VTST:M06-2X-D3/jun-cc-pV(T+d)Z level is −302 K, in good agreement with the experiment.

Another remarkable feature of Figure 7 is that the CCSD(T) calculations in conjunction with a triple-zeta basis set fail to reproduce the temperature behavior of the most recent experiments, which is instead quite well reproduced both by CBS-QB3 and M06-2X-D3. At any rate, better experimental

Table 6. Rate Coefficients at 300 K (in cm^3 $molecule^{-1}$ s^{-1}) for Reaction R1a of Scheme 1 Obtained with Different Methods Employed for Calculating the Geometries and the Associated Energies

single point energy	structure/frequencies	kinetics	well	K_{eq} [a]	TS	barrier	k_{for}	$k_{1a} = k_{for}/K_{eq}$ [b]
CCSD(T)/cc-pVTZ	ωB97X-D/cc-pVTZ	VTST	−4.11	1.41×10^{21}	1.06	5.17	1.85×10^{8}	0.13×10^{-12} (0.07×10^{-12})
		TST					2.25×10^{8}	0.16×10^{-12} (0.09×10^{-12})
	ωB97X-D/6-31+G(d,p)	VTST	−3.70	1.65×10^{21}	0.91	4.62	3.12×10^{8}	0.19×10^{-12} (0.10×10^{-12})
CCSD(T)/jun-cc-pV(T+d)Z	ωB97X-D/jun-cc-pV(T+d)Z	TST	−3.59	2.20×10^{21}	0.94	4.53	7.49×10^{8}	0.34×10^{-12} (0.20×10^{-12})
ωB97X-D/6-31+G(d,p)	ωB97X-D/6-31+G(d,p)	VTST	−4.36	5.49×10^{20}	−2.00	2.35	2.39×10^{10}	43.60×10^{-12} (83.92×10^{-12})
ωB97X-D/cc-pVTZ	ωB97X-D/cc-pVTZ	VTST	−4.43	8.22×10^{20}	−2.42	2.00	3.10×10^{10}	37.70×10^{-12} (78.53×10^{-12})
ωB97X-D/jun-cc-pV(T+d)Z	ωB97X-D/jun-cc-pV(T+d)Z	VTST	−4.01	1.09×10^{21}	−1.80	2.21	2.00×10^{10}	18.40×10^{-12} (28.39×10^{-12})
		TST					3.70×10^{10}	34.05×10^{-12} (62.24×10^{-12})
M06-2X-D3/cc-pVTZ	M06-2X-D3/cc-pVTZ	VTST	−4.82	1.56×10^{21}	−1.17	3.65	4.67×10^{9}	3.00×10^{-12} (4.44×10^{-12})
		TST					7.35×10^{9}	4.72×10^{-12} (7.03×10^{-12})
M06-2X-D3/jun-cc-pV(T+d)Z	M06-2X-D3/jun-cc-pV(T+d)Z	TST	−4.08	4.66×10^{21}	−0.73	3.35	1.47×10^{10}	3.16×10^{-12} (3.78×10^{-12})
CBS-QB3		TST	−3.78	4.20×10^{21}	−1.29	2.49	2.62×10^{10}	6.24×10^{-12} (9.50×10^{-12})
G4		TST	−4.01	2.21×10^{21}	−1.90	2.12	3.52×10^{10}	15.9×10^{-12} (31.53×10^{-12})

[a]Referred to the reverse reaction. [b]Numbers in parenthesis correspond to T = 240 K.

https://dx.doi.org/10.1021/acsearthspacechem.9b00306
ACS Earth Space Chem. 2020, 4, 403−419

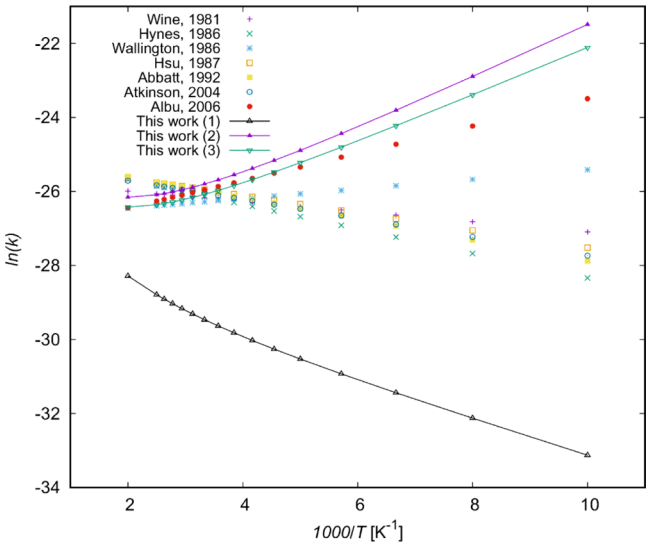

Figure 7. Temperature dependence of the rate coefficient (in cm^3 $molecule^{-1}$ s^{-1}) for reaction R1a according to the equations for experimental determinations present in the literature compared to our own calculations. This work: (1) CCSD(T)/jun-cc-pV(T+d)Z//ωB97X-D/jun-cc-pV(T+d)Z; (2) CBS-QB3; (3) M06-2X-D3/jun-cc-pV(T+d)Z. All curves calculated using CTST.

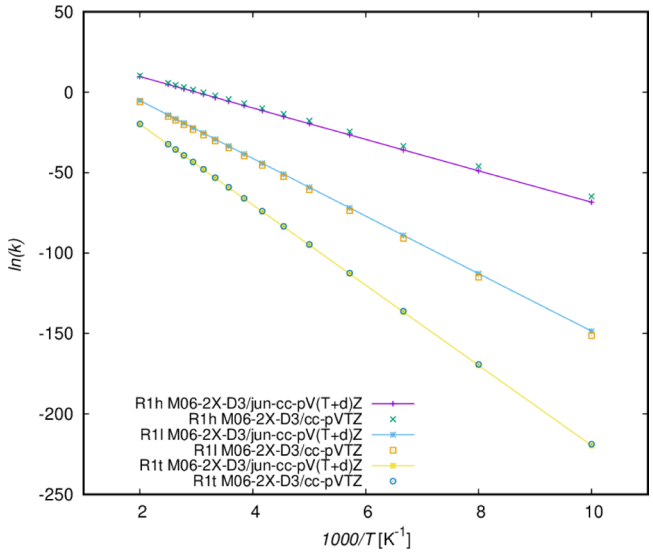

Figure 8. Plot of the dependence of the rate coefficients (in cm^3 $molecule^{-1}$ s^{-1}) of reactions R1h, R1l, and R1t with temperature. All curves calculated using CTST.

measurements and calculations are needed to solve the problem of the temperature dependence for the rate coefficient for pure abstraction in the absence of oxygen. Our results point out that this rate coefficient needs both direct and indirect abstractions to be explained and to show that it is possible to predict accurately (or, at least, in agreement with the best available experimental data) both the rate coefficient at ambient temperature and its temperature dependence.

The same methodology employed to calculate the rate coefficient of R1a was used for reactions R1h, R1l, and R1t, which constitute the final part of our mechanism. In particular, the comparison between R1h and R1l would provide clues about the branching ratio between the more stable MSMOH and the less stable DMSO. These values are collected in Table 7 for several temperatures and plotted in Figure 8.

The comparison of the three rate coefficients shows that reaction R1h will proceed faster than R1l or R1t at any temperature. This means that, as the energy diagram suggested, DMSO will be the preferred product, according to the equation

$$DMS + 2^{\bullet}OH \rightarrow DMSO + H_2O$$

even in the absence of oxygen. This mechanism may be difficult to explore experimentally because if $^{\bullet}OH$ radicals are present in large excess, they may produce oxygen according to the reaction,

$$2^{\bullet}OH \rightarrow H_2O + O$$

and the oxygen atom can interfere with the pure process of abstraction by promoting other oxidation channels. Experimental studies with high $^{\bullet}OH$ concentrations, like those reported by Martin et al.[83] and Nielsen et al.,[23] provided rate coefficients much lower than other experimental determinations, and this failure was attributed to the presence of oxygen impurities that could regenerate hydroxyl radicals.

3.3. Error Evaluation. Calculation of critical points and paths on the PESs and consequently the thermodynamic and kinetic properties of the reactions are subject to unavoidable errors of the methods employed. Therefore, an error analysis should at least be attempted. Notice that we do not have too many experimental data with which to compare. Basically, the experimental data concern the generation of the MTMr radical (for which the reaction energy and the rate coefficient are available) and the enthalpies of formation. For that reason, we

Table 7. Values of the Rate Coefficients (in cm^3 $molecule^{-1}$ s^{-1}) for the Three Reaction Channels R1h, R1l, and R1t

single point energy	structure/frequencies	T (K)	k(R1h)	k(R1l)	k(R1t)
M06-2X-D3/jun-cc-pV(T+d)Z	M06-2X-D3/jun-cc-pV(T+d)Z	200	3.24×10^{-9}	2.15×10^{-26}	5.42×10^{-42}
		240	1.12×10^{-5}	6.75×10^{-20}	6.02×10^{-33}
		300	$\mathbf{3.86 \times 10^{-02}}$	$\mathbf{2.17 \times 10^{-13}}$	$\mathbf{6.89 \times 10^{-24}}$
		400	1.31×10^{2}	7.25×10^{-7}	8.27×10^{-15}
		500	1.70×10^{4}	7.58×10^{-3}	2.38×10^{-9}
barrier (kcal/mol)			*19.2*	*35.2*	*49.3*
M06-2X-D3/cc-pVTZ	M06-2X-D3/cc-pVTZ	200	1.94×10^{-8}	4.64×10^{-27}	7.91×10^{-42}
		240	4.91×10^{-5}	1.77×10^{-20}	8.19×10^{-33}
		300	$\mathbf{12.3 \times 10^{-02}}$	$\mathbf{0.69 \times 10^{-13}}$	$\mathbf{8.76 \times 10^{-24}}$
		400	3.04×10^{2}	2.75×10^{-7}	9.77×10^{-15}
		500	3.26×10^{4}	2.56×10^{-3}	2.71×10^{-9}
barrier (kcal/mol)			*18.5*	*35.8*	*49.1*

https://dx.doi.org/10.1021/acsearthspacechem.9b00306
ACS Earth Space Chem. 2020, 4, 403−419

will focus this discussion on the results collected in Tables 1, 2, and 5. Starting from this last one, one sees that the composite model chemistries are able to reproduce the enthalpies of formation with r.m.s.e smaller than 2.0 kcal/mol and maximum unsigned difference of 2.0 and 3.0 kcal/mol for CBS-QB3 and G4 methods, respectively. This result is not bad but not extremely good either. We have already commented that, contrary to common sense, the least sophisticated model seems to give the best results.

In the case of the PRC2 complex, for which the experimental data afford a stabilization energy of 10.7 ± 2.5 kcal/mol,[21] the DFT values are all within the error bar (see Table 1), no matter the basis set used, and the same happens with the composite model chemistry methods. The CCSD(T) results, however, exhibit strong dependence on both the basis set used and the geometry at which the energy is calculated. While the relative energy $\Delta(E + \mathrm{ZPE})$ of PRC2 at the ωB97X-D level varies by 0.88 kcal/mol (9%), by enlarging the basis set from cc-pVTZ to jun-cc-pV(T+d)Z, the corresponding change becomes 2.4 kcal/mol (46%) at the CCSD(T) level. A smaller variation (11%) is found in the stabilization values of PRC1 and almost no variation for TS0. However, because the TS0 barrier is very low (only 0.18 kcal/mol at the G4 level), those small variations are significant and change even the qualitative meaning of TS0, as can be seen in Table 1.

While the errors associated with the thermochemistry of the PES are well understood and reasonably simple to control, the situation concerning rate coefficients is much more involved. A 2−3 kcal/mol error in a theoretical enthalpy of formation or reaction may be comparable to experimental error bars. However, an error of just 3 kcal/mol in the barrier for a transition state translates into a factor of 150 in the rate coefficient. Therefore, it is unreasonable to expect high accuracy in the calculation of rate coefficients, unless a systematic cancellation occurs among the errors associated with basis sets, methods of calculation of the electronic structure, anharmonic and internal rotor effects, and so forth.

A first attempt to perform such an analysis can be based on the results collected in Table 6. It is clear that the net effect of the changes in geometries, energies, and frequencies at different levels of calculation translates into an enormous variation of the rate coefficient. This has not only quantitative implications but also qualitative ones. In fact, if one plots the rate coefficients as a function of the temperature (Figure 7), the results are striking. The more sophisticated (and costly) CCSD(T)/jun-cc-pV(T+d)Z//ωB97X-D/jun-cc-pV(T+d)Z calculation produces a rate coefficient about 21 times smaller than the experimental value at room temperature and with the opposite temperature dependence than that obtained with the other theoretical calculations.

The following general observations can be made. In the first place, the level at which geometries are determined for the calculation of CCSD(T) energies does not have a large impact in the rate coefficient. The same can be said with respect to the use of TST or VTST procedures for obtaining the rate coefficient. CCSD(T) rate coefficients are consistently lower than the experimental values in the three cases studied. In the second place, composite model chemistries (which are approximations to CCSD(T)/CBS) behave in the opposite way: the rate coefficients are larger than the experiment values, and they differ more from the experiment in the case of the more refined G4 model than in the case of CBS-QB3. In the third place, DFT methods are not per se right or wrong (as compared to the experimental value). While the ωB97X-D method affords values which are too large, the M06-2X-D3 functional affords rate coefficients that are very close to the experimental ones.

The above analysis clearly shows that a good agreement between experimental and theoretical calculations is mostly a result of error compensation, especially at the level at which the geometries and frequencies along the path are calculated. In agreement with other studies we have performed, it seems clear that simply increasing the size and complexity of the basis set at the DFT level does not always lead to a better result.[84] Each density functional seems to have a certain range of basis sets on which it performs optimally because of error compensation. Extending the basis set beyond that point, although appealing from a CBS point of view, does actually worsen the results. While one can judge which is the best level to use in problems where experimental results are known, this task is much more difficult for the rate coefficients for new reactions. In the case of species with several non-hydrogen atoms, for which extremely precise calculations are impossible, the best that can be done is to use consistently the methods that reproduce better the few experimental results that may be available for parts of the system: we followed exactly this approach in the present study.

4. CONCLUSIONS

The field of reactive sulfur intermediates has been blossoming in recent years, and it impacts atmospheric and interstellar chemistry as well as other areas of research. We have studied theoretically in this paper the multigenerational reaction of DMS with hydroxyl radicals, in order to understand better the process of abstraction. To that end, we studied the system in the absence of oxygen, using DFT, CCSD(T), and composite methods of calculation with several basis sets, mimicking in that way experiments performed in reaction chambers. The thermodynamic approach to determine the mechanism and the probable routes was complemented with a calculation of rate coefficients using both CTST and VTST for the most important steps in the mechanism.

From the thermochemical point of view, it was shown that the reaction of abstraction proceeds through a prereactive complex which is different from that of addition, which normally leads to DMSO through reaction with molecular oxygen. The complicated relation between these two minima was studied, and the shape of the portion of the PES that relates them was determined. The subsequent product from abstraction, MTMr, was analyzed, and the main thermochemical characteristics determined with our theoretical results are comparable favorably to the experimental information. It was found that MTMr can evolve according to different channels, depending on the concentration of hydroxyl radicals. The most favorable route, according to the calculations, leads to a seldom explored closed-shell molecule, SMMSA, where the hydroxyl is bound to sulfur. This species can evolve to DMSO by a hydrogen shift from oxygen to carbon or to MSMOH by OH shift from sulfur to carbon. Even if MSMOH is several kcal/mol more stable than SMMSA and DMSO, the height of the barriers for the reactions suggests that DMSO would be the favored product.

Determination of the rate coefficients for the abstraction reaction itself allowed to demonstrate the strengths and weaknesses of the methods used. On the one side, it was shown that it is not necessary to adopt the point of view that

https://dx.doi.org/10.1021/acsearthspacechem.9b00306
ACS Earth Space Chem. 2020, 4, 403−419

indirect H-abstraction starting from the addition complex is necessary to explain the results. Starting from the correct prereactive complex for abstraction and calculating the rate coefficient, we obtained values in the range [3.00−4.72] × 10^{-12} cm^3 $molecule^{-1}$ s^{-1}, in excellent agreement with the most recent value of 4.13 × 10^{-12} cm^3 $molecule^{-1}$ s^{-1} at 298 K. Moreover, we were able to show that the temperature dependence of the rate coefficient follows an inverse Arrhenius behavior, in agreement also with the most recent experimental determination reported by Albu, Barnes et al.[16] and the older one reported by Wallington et al.[32] The negative activation energy obtained from our calculations, −302 K, is also in excellent agreement with the experimentally determined one, −363 ± 27 K, as reported by Albu, Barnes et al.[16] In the light of these facts, we employed our methods to determine also the rate coefficients of the other important reaction channels and confirmed that the reaction leading to DMSO is going to be faster at all temperatures.

The final conclusion of our work is then that DMSO should be obtained also from the abstraction channel provided that enough hydroxyl radicals are available to produce a multi-generational •OH reaction without the need of molecular or atomic oxygen to participate in the process.

■ ASSOCIATED CONTENT

Supporting Information

The Supporting Information is available free of charge at https://pubs.acs.org/doi/10.1021/acsearthspacechem.9b00306.

Notes on the difficulties in the determination of prereactive complexes PRC1 and PRC2, notes on the protocols used to investigate the addition of the second •OH radical to MTM, comparison of the reaction paths using different methods, geometries of all the species reported in this paper at the ωB97X-D/aug-cc-pVQZ level, absolute energies (Hartrees) of intermediates, transition states and products (PDF)

■ AUTHOR INFORMATION

Corresponding Author

Zoi Salta − *SMART Lab, Scuola Normale Superiore, 56126 Pisa, Italy;* orcid.org/0000-0002-7826-0182; Email: Zoi.Salta@sns.it

Authors

Jacopo Lupi − *SMART Lab, Scuola Normale Superiore, 56126 Pisa, Italy;* orcid.org/0000-0001-6522-9947

Vincenzo Barone − *SMART Lab, Scuola Normale Superiore, 56126 Pisa, Italy;* orcid.org/0000-0001-6420-4107

Oscar N. Ventura − *Computational Chemistry and Biology Group, CCBG, DETEMA, Facultad de Química, Udelar, 11200 Montevideo, Uruguay;* orcid.org/0000-0001-5474-0061

Complete contact information is available at: https://pubs.acs.org/10.1021/acsearthspacechem.9b00306

Notes

The authors declare no competing financial interest.

■ ACKNOWLEDGMENTS

This work has been supported by the Italian MIUR (PRIN 2017, project "Physico-chemical Heuristic Approaches: Nano-scale Theory Of Molecular Spectroscopy, PHANTOMS", prot. 2017A4XRCA) and by Scuola Normale Superiore (grant number SNS18_B_TASINATO). The SMART@SNS Laboratory (http://smart.sns.it) is acknowledged for providing high-performance computer facilities. One of the authors acknowledges the continuing financial support of ANII (Uruguay), CSIC (UdelaR), and Pedeciba (Uruguay) for this program of research. Part of the calculations reported in this paper was performed at the Cluster.Uy, the Center for Supercomputing of Uruguay.

■ REFERENCES

(1) Möller, D. Estimation of the global man-made sulphur emission. *Atmos. Environ.* **1984**, *18*, 19−27.

(2) Andreae, M. O.; Ferek, R. J.; Bermond, F.; Byrd, K. P.; Engstrom, R. T.; Hardin, S.; Houmere, P. D.; LeMarrec, F.; Raemdonck, H.; Chatfield, R. B. Dimethyl sulfide in the marine atmosphere. *J. Geophys. Res.* **1985**, *90*, 12891−12900.

(3) Bates, T. S.; Lamb, B. K.; Guenther, A.; Dignon, J.; Stoiber, R. E. Sulfur emissions to the atmosphere from natural sources. *J. Atmos. Chem.* **1992**, *14*, 315−337.

(4) Spiro, P. A.; Jacob, D. J.; Logan, J. A. Global inventory of sulfur emissions with 1°×1° resolution. *J. Geophys. Res.* **1992**, *97*, 6023−6036.

(5) Amels, P.; Elias, H.; Wannowius, K.-J. Kinetics and mechanism of the oxidation of dimethyl sulfide by hydroperoxides in aqueous medium. Study on the potential contribution of liquid-phase oxidation of dimethyl sulfide in the atmosphere. *J. Chem. Soc., Faraday Trans.* **1997**, *93*, 2537−2544.

(6) Yin, F.; Grosjean, D.; Seinfeld, J. H. Photooxidation of dimethyl sulfide and dimethyl disulfide. I: Mechanism development. *J. Atmos. Chem.* **1990**, *11*, 309−364.

(7) Hynes, A. J.; Wine, P. H.; Semmes, D. H. Kinetics and mechanism of OH reactions with organic sulfides. *J. Phys. Chem.* **1986**, *90*, 4148−4156.

(8) Stickel, R. E.; Zhao, Z.; Wine, P. H. Branching ratios for hydrogen transfer in the reactions of OD radicals with CH_3SCH_3 and $CH_3SC_2H_5$. *Chem. Phys. Lett.* **1993**, *212*, 312−318.

(9) Barone, S. B.; Turnipseed, A. A.; Ravishankara, A. R. Role of adducts in the atmospheric oxidation of dimethyl sulfide. *Faraday Discuss.* **1995**, *100*, 39−54.

(10) Yin, F.; Grosjean, D.; Flagan, R. C.; Seinfeld, J. H. Photooxidation of dimethyl sulfide and dimethyl disulfide. II: Mechanism evaluation. *J. Atmos. Chem.* **1990**, *11*, 365−399.

(11) Hatakeyama, S.; Akimoto, H. Reactions of OH radicals with methanethiol, dimethyl sulfide, and dimethyl disulfide in air. *J. Phys. Chem.* **1983**, *87*, 2387−2395.

(12) Hatakeyama, S.; Izumi, K.; Akimoto, H. Yields of SO_2 and formation of aerosol in the photo-oxidation of DMS under atmospheric conditions. *Atmos. Environ.* **1985**, *19*, 135−141.

(13) Barnes, I.; Bastian, V.; Becker, K. H. Kinetics and mechanisms of the reaction of OH radicals with dimethyl sulfide. *Int. J. Chem. Kinet.* **1988**, *20*, 415−431.

(14) Tyndall, G. S.; Ravishankara, A. R. Atmospheric oxidation of reduced sulfur species. *Int. J. Chem. Kinet.* **1991**, *23*, 483−527.

(15) Turnipseed, A. A.; Barone, S. B.; Ravishankara, A. R. Reaction of OH with dimethyl sulfide. 2. Products and mechanisms. *J. Phys. Chem.* **1996**, *100*, 14703−14713.

(16) Albu, M.; Barnes, I.; Becker, K. H.; Patroescu-Klotz, I.; Mocanu, R.; Benter, T. Rate coefficients for the gas-phase reaction of OH radicals with dimethyl sulfide: temperature and O_2 partial pressure dependence. *Phys. Chem. Chem. Phys.* **2006**, *8*, 728−736.

(17) González-García, N.; González-Lafont, À.; Lluch, J. M. Kinetic study on the reaction of OH radical with dimethyl sulfide in the absence of oxygen. *ChemPhysChem* **2007**, *8*, 255−263.

(18) Faloona, I. Sulfur processing in the marine atmospheric boundary layer: A review and critical assessment of modeling uncertainties. *Atmos. Environ.* **2009**, *43*, 2841−2854.

(19) Mardyukov, A.; Schreiner, P. R. Atmospherically relevant radicals derived from the oxidation of dimethyl sulfide. *Acc. Chem. Res.* **2018**, *51*, 475−483.
(20) Barnes, I.; Becker, K. H.; Patroescu, I. FTIR product study of the OH initiated oxidation of dimethyl sulphide: Observation of carbonyl sulphide and dimethyl sulphoxide. *Atmos. Environ.* **1996**, *30*, 1805−1814.
(21) Barone, S. B.; Turnipseed, A. A.; Ravishankara, A. R. Reaction of OH with dimethyl sulfide (DMS). 1. Equilibrium constant for OH + DMS reaction and the kinetics of the OH-DMS + O_2 reaction. *J. Phys. Chem.* **1996**, *100*, 14694−14702.
(22) Barnes, I.; Hjorth, J.; Mihalopoulos, N. Dimethyl sulfide and dimethyl sulfoxide and their oxidation in the atmosphere. *Chem. Rev.* **2006**, *106*, 940−975.
(23) Nielsen, O. J.; Sidebottom, H. W.; Nelson, L.; Treacy, J. J.; O'farrell, D. J. An absolute and relative rate study of the reaction of oh radicals with dimethyl sulfide. *Int. J. Chem. Kinet.* **1989**, *21*, 1101−1112.
(24) Abbatt, J. P. D.; Fenter, F. F.; Anderson, J. G. High-pressure discharge flow kinetics study of OH + CH_3SCH_3, CH_3SSCH_3 → Products from 297 to 368 K. *J. Phys. Chem.* **1992**, *96*, 1780−1785.
(25) Hynes, A. J.; Stoker, R. B.; Pounds, A. J.; Mckay, T.; Bradshaw, J. D.; Nicovich, J. M.; Wine, P. H. A mechanistic study of the reaction of OH with dimethyl-d_6 sulfide. Direct observation of adduct formation and the kinetics of the adduct reaction with O_2. *J. Phys. Chem.* **1995**, *99*, 16967−16975.
(26) Wine, P. H.; Kreutter, N. M.; Gump, C. A.; Ravishankara, A. R. Kinetics of hydroxyl radical reactions with the atmospheric sulfur compounds hydrogen sulfide, methanethiol, ethanethiol, and dimethyl disulfide. *J. Phys. Chem.* **1981**, *85*, 2660−2665.
(27) Atkinson, R.; Perry, R. A.; Pitts, J. N. Rate constants for the reaction of OH radicals with COS, CS_2 and CH_3SCH_3 over the temperature range 299−430 K. *Chem. Phys. Lett.* **1978**, *54*, 14−18.
(28) Kurylo, M. J. Flash photolysis resonance fluorescence investigation of the reactions of OH radicals with OCS and CS_2. *Chem. Phys. Lett.* **1978**, *58*, 238−242.
(29) Williams, M. B.; Campuzano-Jost, P.; Cossairt, B. M.; Hynes, A. J.; Pounds, A. J. Experimental and theoretical studies of the reaction of the OH radical with alkyl sulfides: 1. Direct observations of the formation of the OH-DMS adduct-pressure dependence of the forward rate of addition and development of a predictive expression at low temperature. *J. Phys. Chem. A* **2007**, *111*, 89−104.
(30) Atkinson, R.; Baulch, D. L.; Cox, R. A.; Hampson, R. F.; Kerr, J. A.; Rossi, M. J.; Troe, J. Evaluated kinetic and photochemical data for atmospheric chemistry: Supplement VI. IUPAC Subcommittee on gas kinetic data evaluation for atmospheric chemistry. *J. Phys. Chem. Ref. Data* **1997**, *26*, 1329−1499.
(31) Hsu, Y.-C.; Chen, D.-S.; Lee, Y.-P. Rate constant for the reaction of OH radicals with dimethyl sulfide. *Int. J. Chem. Kinet.* **1987**, *19*, 1073−1082.
(32) Wallington, T. J.; Atkinson, R.; Tuazon, E. C.; Aschmann, S. M. The reaction of OH radicals with dimethyl sulfide. *Int. J. Chem. Kinet.* **1986**, *18*, 837−846.
(33) El-Nahas, A. M.; Uchimaru, T.; Sugie, M.; Tokuhashi, K.; Sekiya, A. Hydrogen abstraction from dimethyl ether (DME) and dimethyl sulfide (DMS) by OH radical: a computational study. *J. Mol. Struct.* **2005**, *722*, 9−19.
(34) Sekušak, S.; Piecuch, P.; Bartlett, R. J.; Cory, M. G. A general reaction path dual level direct dynamics calculation of the reaction of hydroxyl radical with dimethyl sulfide. *J. Phys. Chem. A* **2000**, *104*, 8779−8786.
(35) Cox, R. A.; Sheppard, D. Reactions of OH radicals with gaseous sulphur compounds. *Nature* **1980**, *284*, 330−331.
(36) Atkinson, R.; Pitts, J. N., Jr.; Aschmann, S. M. Tropospheric reactions of dimethyl sulfide with nitrogen oxide (NO_3) and hydroxyl radicals. *J. Phys. Chem.* **1984**, *88*, 1584−1587.
(37) Ravishankara, A. R.; Rudich, Y.; Talukdar, R.; Barone, S. B. Oxidation of atmospheric reduced sulphur compounds: perspective from laboratory studies. *Philos. Trans. R. Soc. London, Ser. B* **1997**, *352*, 171−182.
(38) Yee, L. D.; Craven, J. S.; Loza, C. L.; Schilling, K. A.; Ng, N. L.; Canagaratna, M. R.; Ziemann, P. J.; Flagan, R. C.; Seinfeld, J. H. Secondary organic aerosol formation from low-NOx photooxidation of dodecane: Evolution of multigeneration gas-phase chemistry and aerosol composition. *J. Phys. Chem. A* **2012**, *116*, 6211−6230.
(39) Piletic, I. R.; Howell, R.; Bartolotti, L. J.; Kleindienst, T. E.; Kaushik, S. M.; Edney, E. O. Multigenerational theoretical study of isoprene peroxy radical 1-5-Hydrogen shift reactions that regenerate HOx radicals and produce highly oxidized molecules. *J. Phys. Chem. A* **2019**, *123*, 906−919.
(40) Whalley, L. K.; Edwards, P. M.; Furneaux, K. L.; Goddard, A.; Ingham, T.; Evans, M. J.; Stone, D.; Hopkins, J. R.; Jones, C. E.; Karunaharan, A.; Lee, J. D.; Lewis, A. C.; Monks, P. S.; Moller, S. J.; Heard, D. E. Quantifying the magnitude of a missing hydroxyl radical source in a tropical rainforest. *Atmos. Chem. Phys.* **2011**, *11*, 7223−7233.
(41) Montgomery, J. A., Jr.; Frisch, M. J.; Ochterski, J. W.; Petersson, G. A. A complete basis set model chemistry. VI. Use of density functional geometries and frequencies. *J. Chem. Phys.* **1999**, *110*, 2822−2827.
(42) Montgomery, J. A., Jr.; Frisch, M. J.; Ochterski, J. W.; Petersson, G. A. A complete basis set model chemistry. VII. Use of the minimum population localization method. *J. Chem. Phys.* **2000**, *112*, 6532−6542.
(43) Curtiss, L. A.; Redfern, P. C.; Raghavachari, K. Gaussian-4 theory. *J. Chem. Phys.* **2007**, *126*, 084108.
(44) Barnes, E. C.; Petersson, G. A.; Montgomery, J. A., Jr.; Frisch, M. J.; Martin, J. M. L. Unrestricted Coupled Cluster and Brueckner Doubles Variations of W1 Theory. *J. Chem. Theory Comput.* **2009**, *5*, 2687−2693.
(45) Schuurman, M. S.; Muir, S. R.; Allen, W. D.; Schaefer, H. F., III Toward subchemical accuracy in computational thermochemistry: Focal point analysis of the heat of formation of NCO and [H, N, C, O] isomers. *J. Chem. Phys.* **2004**, *120*, 11586−11599.
(46) Tajti, A.; Szalay, P. G.; Császár, A. G.; Kállay, M.; Gauss, J.; Valeev, E. F.; Flowers, B. A.; Vázquez, J.; Stanton, J. F. HEAT: High accuracy extrapolated ab initio thermochemistry. *J. Chem. Phys.* **2004**, *121*, 11599−11613.
(47) Zhao, Y.; Truhlar, D. G. The M06 suite of density functionals for main group thermochemistry, thermochemical kinetics, noncovalent interactions, excited states, and transition elements: two new functionals and systematic testing of four M06-class functionals and 12 other functionals. *Theor. Chem. Acc.* **2008**, *120*, 215−241.
(48) Grimme, S.; Antony, J.; Ehrlich, S.; Krieg, H. A consistent and accurate ab initio parametrization of density functional dispersion correction (DFT-D) for the 94 elements H-Pu. *J. Chem. Phys.* **2010**, *132*, 154104.
(49) Chai, J.-D.; Head-Gordon, M. Long-range corrected hybrid density functionals with damped atom−atom dispersion corrections. *Phys. Chem. Chem. Phys.* **2008**, *10*, 6615−6620.
(50) Mardirossian, N.; Head-Gordon, M. Thirty years of density functional theory in computational chemistry: an overview and extensive assessment of 200 density functionals. *Mol. Phys.* **2017**, *115*, 2315−2372.
(51) Wang, N. X.; Wilson, A. K. Density Functional Theory and the Correlation Consistent Basis Sets: The Tight d Effect on HSO and HOS. *J. Phys. Chem. A* **2005**, *109*, 7187−7196.
(52) Papajak, E.; Zheng, J.; Xu, X.; Leverentz, H. R.; Truhlar, D. G. Perspectives on Basis Sets Beautiful: Seasonal Plantings of Diffuse Basis Functions. *J. Chem. Theory Comput.* **2011**, *7*, 3027−3034.
(53) Frisch, M. J.; Trucks, G. W.; Schlegel, H. B.; Scuseria, G. E.; Robb, M. A.; Cheeseman, J. R.; Scalmani, G.; Barone, V.; Mennucci, B.; Petersson, G. A.; et al. *Gaussian 16*, revision C.01; Gaussian, Inc.: Wallingford CT, 2016.
(54) Curtiss, L. A.; Raghavachari, K.; Trucks, G. W.; Pople, J. A. Gaussian-2 theory for molecular energies of first- and second-row compounds. *J. Chem. Phys.* **1991**, *94*, 7221−7230.

(55) Curtiss, L. A.; Raghavachari, K.; Redfern, P. C.; Pople, J. A. Assessment of Gaussian-2 and density functional theories for the computation of enthalpies of formation. *J. Chem. Phys.* **1997**, *106*, 1063−1079.
(56) Barker, J. R. Multiple-Well, Multiple-Path Unimolecular Reaction Systems. I. MultiWell Computer Program Suite. *Int. J. Chem. Kinet.* **2001**, *33*, 232−245.
(57) Barker, J. R. Energy Transfer in Master Equation Simulations: A New Approach. *Int. J. Chem. Kinet.* **2009**, *41*, 748−763.
(58) Barker, J. R.; Nguyen, T. L.; Stanton, J. F.; Aieta, C.; Ceotto, M.; Gabas, F.; Kumar, T. J. D.; Li, C. G. L.; Lohr, L. L.; Maranzana, A.; Ortiz, N. F.; Preses, J. M.; Simmie, J. M.; Sonk, J. A.; Stimac, P. J. *Multiwell-2017 Software Suite*; University of Michigan: Ann Arbor, Michigan, USA, 2017, http://claspresearch.engin.umich.edu/multiwell/.
(59) Truhlar, D. G.; Garrett, B. C. Variational Transition State Theory. *Annu. Rev. Phys. Chem.* **1984**, *35*, 159−189.
(60) Baboul, A. G.; Schlegel, H. B. Improved method for calculating projected frequencies along a reaction path. *J. Chem. Phys.* **1997**, *107*, 9413−9417.
(61) Aloisio, S. Theoretical study of adducts of dimethyl sulfide with hydroperoxyl and hydroxyl radicals. *Chem. Phys.* **2006**, *326*, 335−343.
(62) Wang, L.; Zhang, J. Addition complexes of dimethyl sulfide (DMS) and OH radical and their reaction with O_2 by ab initio and density functional theory. *J. Mol. Struct.* **2001**, *543*, 167−175.
(63) Kuhns, D. W.; Tran, T. B.; Shaffer, S. A.; Turecek, F. Methylthiomethyl Radical. A Variable-Time Neutralization-Reionization and ab Initio Study. *J. Phys. Chem.* **1994**, *98*, 4845−4853.
(64) Aloisio, S.; Francisco, J. S. Radical−Water Complexes in Earth's Atmosphere. *Acc. Chem. Res.* **2000**, *33*, 825−830.
(65) Dozova, N.; Krim, L.; Alikhani, M. E.; Lacome, N. Vibrational Spectra and Structures of H_2O−NO, HDO−NO, and D_2O−NO Complexes. An IR Matrix Isolation and DFT Study. *J. Phys. Chem. A* **2006**, *110*, 11617−11626.
(66) Cao, Q.; Berski, S.; Räsänen, M.; Latajka, Z.; Khriachtchev, L. Spectroscopic and Computational Characterization of the HCO··· H_2O Complex. *J. Phys. Chem. A* **2013**, *117*, 4385−4393.
(67) Kumar, M.; Sinha, A.; Francisco, J. S. Role of Double Hydrogen Atom Transfer Reactions in Atmospheric Chemistry. *Acc. Chem. Res.* **2016**, *49*, 877−883.
(68) Hamilton, E. J., Jr.; Lii, R.-R. The dependence on water and on ammonia of the kinetics of the self-reaction of hydroperoxo radical in the gas-phase formation of hydroperoxowater and hydroperoxoammonia complexes. *Int. J. Chem. Kinet.* **1977**, *9*, 875−885.
(69) Salta, Z.; Lupi, J.; Tasinato, N.; Barone, V.; Ventura, O. N. Unraveling the role of additional OH-radicals in the H-Abstraction from Dimethyl Sulfide using Quantum Chemical Computations. *Chem. Phys. Lett.* **2020**, *739*, 136963.
(70) Lan, Y.; Wheeler, S. E.; Houk, K. N. Extraordinary Difference in Reactivity of Ozone (OOO) and Sulfur Dioxide (OSO): A Theoretical Study. *J. Chem. Theor. Comput.* **2011**, *7*, 2104−2111.
(71) Chen, G.; Davis, D. D.; Kasibhatla, P.; Bandy, A. R.; Thornton, D. C.; Huebert, B. J.; Clarke, A. D.; Blomquist, B. W. A Study of DMS Oxidation in the Tropics: Comparison of Christmas Island Field Observations of DMS, SO_2, and DMSO with Model Simulations. *J. Atmos. Chem.* **2000**, *37*, 137−160.
(72) Atkinson, R.; Baulch, D. L.; Cox, R. A.; Crowley, J. N.; Hampson, R. F.; Hynes, R. G.; Jenkin, M. E.; Rossi, M. J.; Troe, J. Evaluated kinetic and photochemical data for atmospheric chemistry: Part 1: gas phase reactions of Ox, HOx, NOx and SOx species. *Atmos. Chem. Phys. Discuss.* **2003**, *3*, 6179−6699.
(73) Shum, L. G. S.; Benson, S. W. Iodine catalyzed pyrolysis of dimethyl sulfide. Heats of formation of CH_3SCH_2I, the CH_3SCH_2 radical, and the pibond energy in CH_2S. *Int. J. Chem. Kinet.* **1985**, *17*, 277−292.
(74) Katoshevski, D.; Nenes, A.; Seinfeld, J. H. A study of processes that govern the maintenance of aerosols in the marine boundary layer. *J. Aerosol Sci.* **1999**, *30*, 503−532.
(75) Chase, M. W., Jr. NIST-JANAF Themochemical Tables, Fourth Edition. *J. Phys. Chem. Ref. Data, Monograph* **1998**, *9*, 1−1951.
(76) Good, W. D.; Lacina, J. L.; McCullough, J. P. Methanethiol and carbon disulfide: Heats of combustion and formation by rotating-bomb calorimetry. *J. Phys. Chem.* **1961**, *65*, 2229−2231.
(77) Ruscic, B.; Berkowitz, J. Photoionization mass spectrometry of CH2S and HCS. *J. Chem. Phys.* **1993**, *98*, 2568−2579.
(78) Sunner, S. Corrected heat of combustion and formation values for a number of organic sulphur compounds. *Acta Chem. Scand.* **1963**, *17*, 728−730.
(79) DeMore, W. B.; Sander, S. P.; Golden, D. M.; Hampson, R. F.; Kurylo, M. J.; Howard, C. J.; Ravishankara, A. R.; Kolb, C. E.; Molina, M. J. *Chemical Kinetics and Photochemical Data for Use in Stratospheric Modeling*; JPL Publication 97-4, 1997; p 1.
(80) Atkinson, R. Kinetics and mechanisms of the gas-phase reactions of the hydroxyl radical with organic compounds. *J. Phys. Chem. Ref. Data, Monograph* No. *1*, **1989**.
(81) Williams, M. B.; Campuzano-Jost, P.; Hynes, A. J.; Pounds, A. J. Experimental and theoretical studies of the reaction of the OH radical with alkyl sulfides: 3. Kinetics and mechanism of the OH initiated oxidation of dimethyl, dipropyl, and dibutyl sulfides: reactivity trends in the alkyl sulfides and development of a predictive expression for the reaction of OH with DMS. *J. Phys. Chem. A* **2009**, *113*, 6697−6709.
(82) Atkinson, R.; Baulch, D. L.; Cox, R. A.; Crowley, J. N.; Hampson, R. F.; Hynes, R. G.; Jenkin, M. E.; Rossi, M. J.; Troe, J. Evaluated kinetic and photochemical data for atmospheric chemistry: Volume I - gas phase reactions of Ox, HOx, NOx and SOx species. *Atmos. Chem. Phys.* **2004**, *4*, 1461−1738.
(83) Martin, D.; Jourdain, J. L.; LeBras, G. Kinetic study for the reactions of OH radicals with dimethylsulfide, diethylsulfide, tetrahydrothiophene, and thiophene. *Int. J. Chem. Kinet.* **1985**, *17*, 1247−1261.
(84) Irving, K.; Kieninger, M.; Ventura, O. N. Basis Set Effects in the Description of the Cl-O Bond in ClO and XClO/ClOX Isomers (X= H, O, and Cl) Using DFT and CCSD (T) Methods. *J. Chem.* **2019**, *2019*, 4057848.